

Angle of Incidence  
And  
Power Degradation Analysis of Photovoltaic Modules

by

Suryanarayana Vasantha Janakeeraman

A Thesis Presented in Partial Fulfillment  
of the Requirements for the Degree  
Master of Science in Technology

Approved April 2013 by the  
Graduate Supervisory Committee:

Govindasamy Tamizhmani, Chair  
Bradley Rogers  
Narciso Macia

ARIZONA STATE UNIVERSITY

May 2013

## **ABSTRACT**

Photovoltaic (PV) module nameplates typically provide the module's electrical characteristics at standard test conditions (STC). The STC conditions are: irradiance of 1000 W/m<sup>2</sup>, cell temperature of 25°C and sunlight spectrum at air mass 1.5. However, modules in the field experience a wide range of environmental conditions which affect their electrical characteristics and render the nameplate data insufficient in determining a module's overall, actual field performance. To make sound technical and financial decisions, designers and investors need additional performance data to determine the energy produced by modules operating under various field conditions. The angle of incidence (AOI) of sunlight on PV modules is one of the major parameters which dictate the amount of light reaching the solar cells. The experiment was carried out at the Arizona State University- Photovoltaic Reliability Laboratory (ASU-PRL). The data obtained was processed in accordance with the IEC 61853-2 model to obtain relative optical response of the modules (response which does not include the cosine effect). The results were then compared with theoretical models for air-glass interface and also with the empirical model developed by Sandia National Laboratories. The results showed that all modules with glass as the superstrate had identical optical response and were in agreement with both the IEC 61853-2 model and other theoretical and empirical models.

The performance degradation of module over years of exposure in the field is dependent upon factors such as environmental conditions, system configuration, etc. Analyzing the degradation of power and other related performance parameters over time will provide vital information regarding possible degradation rates and mechanisms of the modules. An extensive study was conducted by previous ASU-PRL students on approximately 1700 modules which have over 13 years of hot- dry climatic field condition. An analysis of the results obtained in previous ASU-PRL studies show that the major degradation in crystalline silicon modules having glass/polymer construction is encapsulant discoloration (causing short circuit current drop) and solder bond degradation (causing fill factor drop due to series resistance increase). The power

degradation for crystalline silicon modules having glass/glass construction was primarily attributed to encapsulant delamination (causing open-circuit voltage drop).

## **DEDICATION**

I would like to dedicate my thesis to my beloved parents, relatives, and friends in India. It is only because of their constant support and motivation that I am here today.

## **ACKNOWLEDGMENTS**

First, I would like to convey my heartfelt thanks to Dr.Govindasamy TamizhMani for his constant guidance and support throughout the project. I would also like to thank Dr.Bradley Rogers and Dr.Narciso Macia for readily accepting to be on my advising committee. In addition, I owe thanks to Mr.Joseph Kuitche, PRL Lab Manager. His suggestions and cooperation played an important role in analyzing the results. I will be forever grateful to my colleague and friend Mr.Brett Knisely for his support and motivation through the course of my project. I would to like thank former PRL students, Mr.Faraz Ebneali, Ms.Qurat-ul-Ain Shah (Annie), Mrs.Meena Gupta Vemula, Mr.Sai Tatapudi, Mr.Kolapo Olakonu, Mrs. Liliyang Yan (Cassie), Mr.Jaspreet Singh, Mr.Kartheek Koka for treating me like a younger brother and constantly guiding me. I would also like to thank current PRL students, Mr.Cameron Anderson, Mr.Jonathan Belmont, Mr.Jayakrishna Mallineni and Mr.Karan Rao Yedidi. Last but not the least, I would like to thank my friends Mr.Lalith, Mr.Krishna, Mr. Aravind, Mr.Sai Rajagopal, Mr.Vignesh, Mr.Anand Chari, Mr.Siddharth Kulasekaran, Mr.Shrinidhi Iyengar, Mr.Dilip Ramani and Mr.Prashanth Ganeshram for their constant support.

## TABLE OF CONTENTS

	Page
LIST OF TABLES .....	vii
LIST OF FIGURES .....	viii
CHAPTER	
1. INTRODUCTION .....	1
1.1 Background .....	1
1.2 Statement of Problem .....	1
1.3 Scope and Purpose of the Project .....	2
2. LITERATURE REVIEW .....	3
3. EXPERIMENTAL METHODS .....	6
3.1 Measurement with calibrated pyranometers .....	6
3.2 Outdoor Measurement Procedure of ASU-PRL .....	8
3.3 Methodology for Power plant analysis .....	13
3.4 Statistical Hypothesis Testing using Minitab Software .....	15
4. RESULTS AND DISCUSSION .....	17
4.1 Relative $I_{sc}$ with diffused component and cosine effects .....	17
4.2 Relative $I_{sc}$ without diffused component and cosine effects .....	17
4.3 Comparison between the models .....	21
4.4 Uncertainty Analysis .....	22
4.5 Results and Discussions for Power Plant Analysis .....	23
5. CONCLUSIONS .....	31
REFERENCES .....	33
APPENDIX	
A SANDIA PROCEDURE TO DETERMINE RELATIVE OPTICAL RESPONSE $f_2(AOI)$ .....	34
B CROSSCHECKING OF AOI DEVICE USING MANUAL METHOD .....	40

APPENDIX	Page
C ROUND 1: MEASUREMENTS USING A MULTI-CURVE TRACER.....	44
D ROUND 2: MEASUREMENTS USING A TRANSDUCERS AND DATA LOGGER .....	48
E INTER-COMPARISON AND CROSSCHECKING OF PYRANOMETERS .....	51
F MEASUREMENT OF $f_2$ (AOI) VERSES AOI IN THE OPPOSITE DIRECTION.....	56
G GRAPHICAL METHOD FOR FINDING THE PARAMETER CAUSING DROP IN POWER.....	61
H PARETO CHART OF DEFECTS IN MODULES FOR EACH TYPE OF MODEL .....	66
I ANNUAL AVERAGE DEGRADATION RATE FOR I-V PARAMETERS FOR ALL MODELS .....	71
J HISTOGRAMS OF POWER DEGRADATION FOR VARIOUS MODELS.....	76
K SAMPLE HYPOTHESIS TESTING USING MINITAB SOFTWARE .....	81

## LIST OF TABLES

Table .....	Page
1. Model designation and module counts in power plant .....	14
2. Uncertainty of various uncertainty contributors in equations 4 and 5.....	22
3. Values for mean and median for each model.....	25
4. Primary parameter and the primary visual defect causing the degradation in power for each model .....	29
E1.Comparison of Kipp & Zonen CMP21 verses Eppley PSP measured global irradiance in the plane of array for 87% direct to global irradiance ratio .....	53



## LIST OF FIGURES

Figure .....	Page
1: (A) DC current transducers; (B) CR 1000 DAS with a multiplexer .....	10
2: (A) AOI device; (B) AOI device mounted on a plastic arm .....	10
3: (A) Sundial 'zeroed' to AOI platform with no shadow present; B) AOI accuracy check on mono-Si module using the sundial.....	11
4: Angle of incidence measurement setup on a two-axis tracker.....	11
5: Pictures of all models in APS-STAR power plant.....	14
6: Relative $I_{sc}$ with diffused component and cosine effects .....	17
7: Relative $I_{sc}$ without diffused component and cosine effects – IEC method .....	19
8: Relative $I_{sc}$ without diffused component and cosine effects – Sandia method .....	19
9: Comparison between Eppler and Kipp & Zonen pyranometers – CdTe Module.....	20
10: Comparison between various models developed by different institutions .....	21
11: Uncertainties obtained as error bars presented for all modules.....	23
12: Plot for I-V Parameters versus average annual degradation rates for all models.....	23
13: Histogram of degradation rates .....	24
14: Power Mean and Median for various models .....	25
15: Plot for various I-V parameter degradation (%/year) for Model A13 .....	26
16: Plot for various I-V parameter degradation (%/year) for Model B .....	26
17: Plot for various I-V parameter degradation (%/year) for Model C12 .....	27
18: Plot for various I-V parameter degradation (%/year) for Model D .....	27
19: Plot for various I-V parameter degradation (%/year) for Model E .....	28
20: Plot for various I-V parameter degradation (%/year) for Model F .....	28
21: Plot for various I-V parameter degradation (%/year) for Model C4 .....	29
A 1: Empirical $f_2$ (AOI) measurements by Sandia National Laboratories for conventional flat-plate modules with a planar glass front surfaces. ....	38

Figure.....	Page
B 1:Comparison of relative optical responses obtained using the AOI hardware and AOI calculation for a CdTe module with glass superstrate for azimuth rotation(direct to global ratio was 0.89).....	42
B 2:Comparison of relative optical responses obtained using the AOI hardware and AOI calculation for a CdTe module with glass superstrate for elevation rotation (direct to global ratio was 0.89) .....	42
C 1:Round 1 – Relative short circuit current verses AOI for five modules (Multi-curve tracer method) .....	46
C 2:Round 1 - Data for five modules where $f_2(\text{AOI})$ was <i>erroneously</i> calculated using Equation A6 (Multi-curve tracer method) .....	47
D 1:Round 2 - Relative short circuit current verses AOI for five modules (Data logger method).....	49
D 2:Round 2 - Data for five modules where $f_2(\text{AOI})$ was <i>correctly</i> calculated using Equation A6 (Data logger method).....	50
E 1:Global irradiance as measured by the Kipp & Zonen CMP21 and Eppley PSP pyranometer for 87% Edni/Epoa .....	52
E 2:Comparison of Kipp & Zonen CMP21 verses Eppley PSP measured global irradiance in the plane of array for 81% direct to global irradiance ratio .....	54
E 3:Comparison of Kipp & Zonen CMP21 verses Eppley PSP measured global irradiance in the plane of array for 2% direct to global irradiance ratio .....	55
F 1:Round 3 - Data for five modules where $f_2(\text{AOI})$ was calculated when the tracker was rotated in the opposite direction (East to West).....	57
F 2:Round 3 - Data for $f_2(\text{AOI})$ calculated for CdTe from West to East compared to data when the tracker was rotated in the opposite direction (East to West).....	58
F 3:Round 3 - Data for $f_2(\text{AOI})$ calculated for a-Si from West to East compared to data when the tracker was rotated in the opposite direction (East to West) .....	58

Figure.....	Page
F 4: Round 3 - Data for $f_2(\text{AOI})$ calculated for CIGS from West to East compared to data when the tracker was rotated in the opposite direction (East to West).....	59
F 5: Round 3 - Data for $f_2(\text{AOI})$ calculated for Mono-Si from West to East compared to data when the tracker was rotated in the opposite direction (East to West).....	59
F 6: Round 3 - Data for $f_2(\text{AOI})$ calculated for Poly-Si from West to East compared to data when the tracker was rotated in the opposite direction (East to West).....	60
G 1: Degradation power versus degradation of I-V parameters for model A13 .....	62
G 2: Degradation power versus degradation of I-V parameters for Model B .....	62
G 3: Degradation power versus degradation of I-V parameters for model C12.....	63
G 4: Degradation power versus degradation of I-V parameters for Model C4.....	63
G 5: Degradation power versus degradation of I-V parameters for Model D .....	64
G 6: Degradation power versus degradation of I-V parameters for Model E .....	64
G 7: Degradation power versus degradation of I-V parameters for Model F .....	65
H 1: Pareto chart of defects for Model A13 .....	67
H 2: Pareto chart of defects for Model B .....	67
H 3: Pareto chart of defects for Model C12 .....	68
H 4: Pareto chart of defects for Model C4 .....	68
H 5: Pareto chart of defects for Model D .....	69
H 6: Pareto chart of defects for Model E .....	69
H 7: Pareto chart of defects for Model F .....	70
I 1: Plot for average annual degradation of I-V parameters for Model A13.....	72
I 2: Plot for average annual degradation of I-V parameters for Model B.....	72
I 3: Plot for average annual degradation of I-V parameters for Model C12 .....	73
I 4: Plot for average annual degradation of I-V parameters for Model C4 .....	73
I 5: Plot for average annual degradation of I-V parameters for Model D .....	74
I 6: Plot for average annual degradation of I-V parameters for Model E.....	74

Figure.....	Page
I 7: Plot for average annual degradation of I-V parameters for Model F .....	75
J 1: Histogram of Power Degradation (%/Year) for Model A13.....	77
J 3: Histogram of Power Degradation (%/Year) for Model B.....	77
J 4: Histogram of Power Degradation (%/Year) for Model C12 .....	78
J 5: Histogram of Power Degradation (%/Year) for Model C4 .....	78
J 6: Histogram of Power Degradation (%/Year) for Model D .....	79
J 7: Histogram of Power Degradation (%/Year) for Model E.....	79
J 8: Histogram of Power Degradation (%/Year) for Model F .....	80
K 1: Degradation values of $I_{sc}$ , $V_{oc}$ and Fill Factor per year pasted on Minitab .....	82
K 3: Options button for performing 2 Sample t test in Minitab.....	82
K 4: Samples placed on two different columns in the dialog box are compared.....	83
K 5: A symbol chosen for implementing the alternative hypothesis .....	83
K 6: Window containing the P-Value .....	84

## Chapter 1

### 1. INTRODUCTION

#### 1.1 Background

The angle of Incidence (AOI) of a PV module can be defined as the angle between the incident beam of light and a line perpendicular to the plane of the module. Light entering the module has to pass through a glass cover, encapsulant layer, and an antireflective coating layer before reaching the energy producing material of the solar cell. Photovoltaic module ratings provided by the manufacturers are performed at STC conditions, with irradiance being  $1000 \text{ W/m}^2$ ,  $25^\circ\text{C}$  cell temperature. These ratings are measured at an incident angle of  $0^\circ$ , whereas in an actual field, the angle of incidence varies resulting in higher losses than the rated values. This simply implies that for AOI values greater than zero, the module's performance will be lower than the one rated at STC conditions. The electrical characteristics of PV modules are affected during such real-time conditions, especially the current (amperes). The first part of this work investigates the influence of AOI on PV modules' performance.

In PV power plants, the average annual power degradation rate is used as one of the primary metrics to determine and predict the total energy produced by the system. The degradation rate is dictated by the module design quality, manufacturing quality, and site-specific environmental conditions. The power degradation could be attributed to one or more of the performance parameters: current, voltage or fill factor. The second part of this thesis investigates the distribution of these performance parameters which influence the power degradation of PV modules.

#### 1.2 Statement of Problem

The main objective of the first part is to test and validate the IEC 61853-2 (draft) standard procedure for measuring the effect of AOI on PV modules. The following statement from IEC 61853-2 "for the flat glass superstrate modules, the AOI test does not need to be performed;

*rather, the data of a flat glass air interface can be used*", needs to be validated by comparing the plots obtained from the IEC 61853-2 model complying with those plots obtained using theoretical and empirical models. The relative light transmission plots for all modules with glass superstrates should be identical.

The main purpose of the second part of the thesis is to:

- To check whether the modules degraded at a constant rate or at a highly varied rate by the means of statistical analysis.
- Statistically analyze the possible visual factors that cause power degradation.

### **1.3 Scope and Purpose of the Project**

Due to the short project period available to execute this labor intensive project, this project was carried out jointly in collaboration with another MS thesis student, Brett Knisely. The scope of the first part of this thesis and Mr. Knisely's thesis is to test and validate AOI test methods and models identified in draft standard IEC 61853-2. Mr. Knisely's thesis is expected to be submitted in summer 2013 and will uniquely focus on the quantum efficiency of PV module cells. The second part of this thesis will uniquely focus on analyzing a power plant and determining the major factors causing degradation in power. The current-voltage (I-V) data obtained by previous researchers of ASU-PRL was analyzed and distributions of power degradation in power per year were plotted for each model. Additionally, degradations in the  $I_{SC}$ ,  $V_{OC}$  and fill factor (FF) per year were obtained using statistical hypothesis testing.

## Chapter 2

### 2. LITERATURE REVIEW

The PV industry currently aims to evaluate modules beyond STC conditions by studying the factors affecting module performance and designing a proper test method for measuring the effects of angles of incidence (AOI). The power generated by the module is directly related to the irradiance incident upon it. Thus, prior research conducted by Sandia National Laboratories determined that two factors which complicate the characterization of modules are: 1) variations in solar spectrum and 2) optical properties with the AOI. Higher angle of incidence considerably lowers the module's power. The performance of a PV module is reported at 1.5 air mass, with air mass characterizing the solar spectrum after sunlight has travelled through the atmosphere. The air mass quantifies the reduction in the amount of light as it passes through the atmosphere and is absorbed by air and dust. When the sun is directly overhead, air mass is a unity. The magnitude of change in the sunlight's spectrum also has a major impact on performance. A procedure for measuring the effect of AOI on the modules was developed using empirical equations. In other studies, researchers had developed an analytical model for finding the annual angular losses due to real-world conditions. This model is a function of tilt, location, and season, and concurs with the model developed by previous researchers. The amount of sunlight reaching the solar cells is dependent upon the reflected and transmitted fractions of incident light. The following two module design elements influence module performance, 1) transmittance (light passing through the superstrate, and encapsulant), and 2) reflectance (scattered light bouncing through and around the: superstrate and encapsulant, the air/superstrate, and encapsulant/cell interfaces. These are a function of AOI. The effect of AOI is heavily dependent upon the surface roughness and the antireflective coatings of the superstrate.

The short circuit current of a PV module is affected by: the mechanical/geometrical effect and the optical effect. The geometrical effect is best described as the orientation of the module with respect to incident light. The geometrical effect is also known as the cosine effect and states

that the irradiance falling on the module decreases as the AOI increases. The irradiance is directly related to cosine (AOI). The second factor influencing AOI is the optical effects, which describes the surface characteristics of the module. The majority of PV manufacturers constantly research to improve the surface characteristics of modules by modifying the anti-reflective coatings, and/or glass type (rolled or textured glass).

The effects of AOI on short circuit current were tested for five different module technologies: amorphous silicon (a-Si), cadmium telluride (CdTe), copper indium gallium selenide (CIGS), mono crystalline silicon (Mono-Si) and polycrystalline silicon (Poly-Si).

To make a module durable for field use, failure rates needs to be kept low. Reliability studies play a significant role in analyzing and modifying the product for better success in the commercial market. The performance of a module at its rated power for the claimed number of years is the key for reliability studies. After extensive research in reliability, failures during the initial stages of the module's life have been reduced. The failure rate increases rapidly during the final stages of a module's life. Plotting the failure rate with respect to product life would give us a bath tub curve. Module lifetime field testing requires a long time, which is not possible in today's highly competitive world. Increasing stress levels beyond the design limits accelerate failures in the product. This is known as accelerated testing and is employed extensively in the industry. These tests help in identifying and correcting defects which would reduce module mortality rates. Several research studies have analyzed the factors affecting module degradation using historical field data. One such research involved the analysis of 9.2 KWp PV array situated near Trinidad, CA, on the Pacific coast. The average power degradation rate for these modules was found to be decreased by 4.39% after 11 years in the field. The major cause for degradation was due to short circuit current which decreased by 6.38% after 11 years. On analyzing the same array after 20 years in the field, the power drop was found to be 16.13 %. Again, the major factor was found to be current drop due to browning or discoloration of the encapsulant.



The National Renewable Energy Laboratory (NREL) researched 12 different monocrystalline and polycrystalline modules and found that the modules degraded less than 0.5 % per year with the main cause of power degradation being a drop in short circuit current. Another research project performed by NREL on 2000 modules of various technologies found that the degradation rate was less than 1 % per year. The crystalline modules degraded largely due to a drop in the  $I_{SC}$  values, and to some extent, the fill factor. The thin film module technologies degraded due to a decline in the fill factor, especially in humid climates. The current research was performed on 1700 crystalline silicon modules which were in hot and dry climatic field conditions for over 13 years.

## Chapter 3

### 3. EXPERIMENTAL METHODS

#### 3.1 Measurement with calibrated pyranometers

During the course of this project, the testing and analysis procedure was performed in three rounds, with the third round resulting in accurate and satisfying data. The data obtained in the third round of testing and analysis is presented in this chapter. The data obtained in the previous two rounds is provided for reference in Appendices C and D of this thesis.

#### **Test Apparatus:**

The following are the types of test apparatus used in the experiment along with a brief description.

- 1) **Irradiance Sensors:** The global and direct irradiances can be measured using these devices. According to the measurement procedure of standard IEC 61853-2 (draft), a combination of pyranometer (for measuring global irradiance) and pyrliometer (for measuring direct normal irradiance) were used.
- 2) **Thermal Sensors:** The ambient, module, and reference cell temperature are measured using T-type thermocouples.
- 3) **Data acquisition system:** A data acquisition system was used to collect and store data from the modules using irradiance and thermal sensors.
- 4) **Two-axis Tracker:** All the test modules were placed on a two axis tracker, so that the azimuth and tilt could be controlled.
- 5) **AOI measuring device:** This device is used to determine the tilt angle as well as to verify the co planarity of test modules and irradiance sensors.

#### **Test Setup:**

- 1) The front surface of the test modules should be thoroughly cleaned.
- 2) The test modules should be mounted on a two-axis tracker securely.

- 3) The test modules and all the sensors should be connected to the data acquisition system.

#### Measurement Procedure:

- 1) If the diffused component does not exceed 10% of the total irradiance, the short circuit current measured ( $I_{sc}(\theta)$ ) can be used to calculate the relative angular light transmission data,  $\tau(\theta)$ . But, if the diffused component exceeds 10% of the total irradiance, then the short circuit current ( $I_{sc}(\theta)$ ) should be corrected for the calculation of  $\tau(\theta)$ . This correction is dependent on the type of sensor used.
- 2) If the irradiance sensor is a reference cell: The diffused component should not be more than 10% of the total irradiance obtained during the measurement of  $I_{sc}(\theta)$ . If the diffused component exceeds 10%, it can be subtracted from global irradiance after measuring the angular response with blocked direct light component or by blocking the diffused component by reducing the field of view of the diffused component.
- 3) If the irradiance sensors are pyranometers and pyrhemimeters: The diffused light striking the module would be given as :

$$G_{diff} = G_{tpoa} - G_{dni} \cos(\theta) \quad (1)$$

Where:

“ $G_{tpoa}$ ” is the total irradiance in the plane of the module, as measured by a pyranometer

“ $G_{dni}$ ” is the direct light component measured by the pyrhemimeter.

“ $\theta$ ” is the tilt angle between the direct irradiance falling on the module and the normal of module.

The short circuit current obtained from direct light component can be obtained from the diffused light component which is given as follows:

$$I_{sc}(\theta) = I_{sc \text{ measured}}(\theta) (1 - G_{diff} / G_{tpoa}) \quad (2)$$

The relative angular light transmission (or relative angular optical response) into the module is given by:

$$\tau(\theta) = I_{sc}(\theta) / (\cos(\theta) I_{sc}(0)) \quad (3)$$

### 3.2 Outdoor Measurement Procedure of ASU-PRL

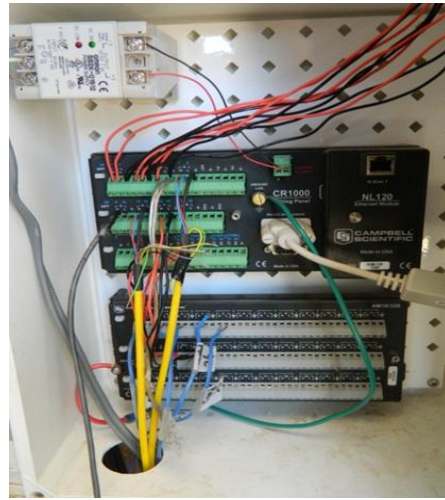
This experiment was performed at ASU-PRL, and the measurements obtained in accordance with standard IEC 61853-2 (draft). The details of the apparatus used in the experiment are given as follows:

- 1) **Test Modules:** Five different technologies were used: monocrystalline silicon (Mono-Si), polycrystalline silicon (Poly-Si), amorphous silicon (a-Si), cadmium telluride (CdTe) and copper indium gallium Selenide (CIGS). Glass was the superstrate in all the cases.
- 2) **Irradiance Sensors:** A reference cell (Poly-Si), two pyranometers from 2 manufacturers namely Eppley PSP and Kipp & Zonen and pyrhelimeter from Kipp & Zonen were used. The data obtained using the pyranometers and pyrhelimeters were later processed.
- 3) **Thermal Sensors:** T-Type thermocouples manufactured by Omega were placed at the centre of the back sheet of the modules with the help of a thermal tape. The accuracy was given to be  $\pm 1^\circ \text{C}$  above  $0^\circ \text{C}$ .
- 4) **Data acquisition system:** CR1000 manufactured by Campbell Scientific was used to collect data. A magnetic DC current transducer (Figure 1A) was used to measure the short circuit current. This equipment is kept in an air conditioned room for maintaining a constant operating temperature. The accuracy of this equipment is 1%. A linear relation was given for the current passing through the transducer and its output voltage. All the data was recorded and stored in the data acquisition system.
- 5) **Two axis tracker:** All the modules, irradiance sensors and the AOI measuring devices were mounted on the two axis tracker. Usually a tracker has full range of motion in order to achieve high angles of incidence during any time of the day. The tracker was limited to  $65^\circ$  of rotation about elevation angle and  $180^\circ$  about the Azimuth angle. Higher AOI was obtained by starting the experiment at approximately 2:30pm (for our setup) so that the full range in azimuth could be utilized. Since the direct irradiance was necessary to be obtained, a pyrhelimeter was allowed to track the sun.

6) **Angle of Incidence measuring device:** In order to find the tilt angle, a 3DM-GX3-25 miniature altitude heading reference system (figure 2A) was used. It is a high performance, miniature altitude reference system and was manufactured by Microstrain. It consists of a triaxial accelerometer, triaxial magnetometer, temperature sensors and a processor that runs an algorithm to give static and dynamic orientation measurements with a manufacturer rated accuracy of  $\pm 0.5^\circ$  static accuracy and a  $\pm 0.2^\circ$  repeatability. In order to comply with the static accuracy of the device, the tracker was stopped for six seconds at each AOI. This allowed for a stable AOI reading from the device. AOI software was used to calculate the position of the sun relative to the modules orientation and the AOI could be obtained. This was placed on the surface of a plastic platform (Figure 2B) at the end of a plastic bar extending from the tracker and AOI data was measured and recorded by a laptop. The tracker was manually rotated along the azimuth and elevation, while referring to the software for AOI. The AOI data and data recorded by the Campbell Scientific CR1000 data logger were combined by synchronizing the laptop's clock to that of the data logger.

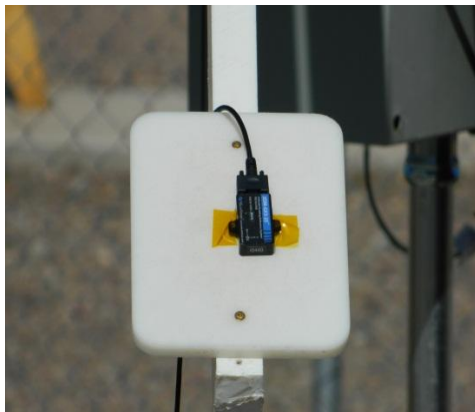


(A)



(B)

Figure 1: (A) DC current transducers; (B) CR 1000 DAS with a multiplexer



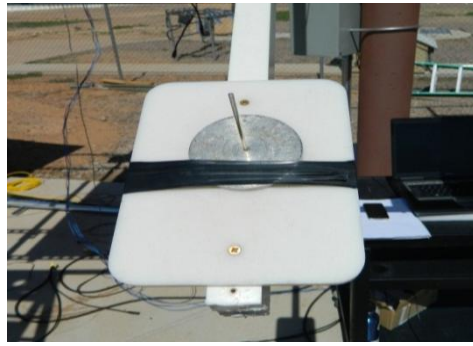
(A)



(B)

Figure 2: (A) AOI device; (B) AOI device mounted on a plastic arm

To ensure that all reference devices and modules are coplanar with respect to each other, the altitude heading device was placed on each module and the AOI could be obtained and checked for consistency. The presence of any magnetic material near the device would marginally affect the accuracy. To check the co-planarity, the tracker was set to automatic mode and was allowed to track at an angle normal to the incident light.



(A)



(B)

Figure 3: (A) Sundial 'zeroed' to AOI platform with no shadow present; (B) AOI accuracy check on mono-Si module using the sun-dial

### Test Setup:

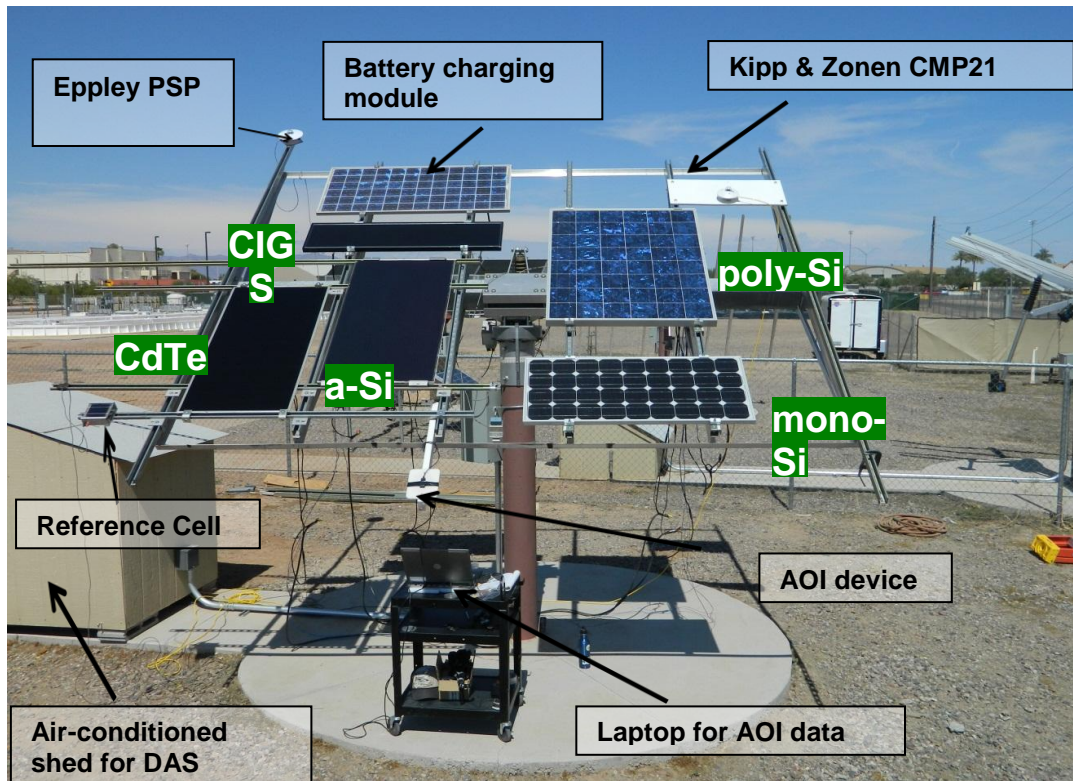


Figure 4: Angle of incidence measurement setup on a two-axis tracker

Both AOI device and the sundial were placed on a small plastic board and the tracker was tuned so that the AOI device read an AOI of  $0.3^\circ$  or lower and also there was no shadow of

the sundial (Figure 3A). Then the sundial was placed on each module at various positions such as center and corner. The shadow was obtained for each position and as shown in the equation below, the point of the tracker with the longest shadow length represented least accurate point with respect to AOI ( $AOI_{\max \text{ error}}$ ). The maximum shadow length was found to be  $0.7^\circ$ . Given that the initial AOI reading was a maximum of  $0.3^\circ$ , the projected maximum uncertainty for was  $\pm 1.0^\circ$ .

### Measurement Procedure

Data was collected as quickly as possible to mitigate the effects due to module temperature and solar spectral variations. The following factors were given primary importance during the experiment.

- 1) **Soiling:** Dust can be a major influence on the irradiance reaching the module's surface. The modules were cleaned before data collection.
- 2) **Reflection from surroundings:** Items or objects of high reflectance should not be present when the data is being collected. No significant reflections were observed in the surroundings. Protruding devices were removed from the tracker and the ground was a flat gravel surface.
- 3) **Standard and constant irradiance:** The experiment was performed during clear sky conditions when the ratio of direct normal irradiance to the global normal irradiance was greater than 0.85. This ratio is a major factor during the measurement, especially at higher AOI.
- 4) **Standard and constant spectrum:** Ideally, the experiment must be performed during solar noon to reduce the effect of spectral variation during the test period. Since there was limitation with the tracker movements, the test was performed around 2:30 pm to utilize the full range of the tracker. However, the test was completed in 10 minutes so that a constant spectrum could be maintained throughout the experiment. The AOI was varied by moving the tracker in azimuth and elevation from west to east to angles close to  $90^\circ$ .



- 5) **Standard and constant temperature:** The measurements should be done at a constant module temperature. But, when the AOI varies, the modules' temperature varies because of changes in the irradiance. A thermocouple was placed on the back sheet of the modules and the temperature was recorded throughout the experiment. From the temperature coefficient obtained while taking baselines for each module, the short circuit current was corrected for 25°C to remove the influence of varying temperature during the experiment.
- 6) **Maximum number of data points:** The larger the data collected, higher the accuracy of the measurements. The data logger collected data at a frequency of 30 seconds, and a large amount of data was collected to increase the accuracy of measurements. To obtain data with nearly constant irradiance and air mass conditions, the tracker was moved 5° every 30 seconds up to AOI close to 85° (or as far as the tracker would allow). Hence the  $I_{sc}$  vs. AOI graph was plotted with a minimum of 18 data points.

### 3.3 Methodology for Power plant analysis

The I-V data collected for 1900 modules at the power plant was translated to STC conditions by a procedure developed at the Arizona State University. Table 1 shows the module models and the physical characteristics of the power plant array. In order to not disclose the names of the module manufacturers, the modules were given model names from A to F. Model A and F are further segregated based on the number of years in the field. The figure 5, shows the different models analyzed at the power plant.

Table 1: Model designation and module counts in power plant

Model designation and module count								
Array	Model A18	Model A13	Model B	Model C12	Model C4	Model D	Model E	Model F
Size	11.6 kW	9 kW	81.9 kW	51.3 kW	51.3 kW	12 kW	8.8 kW	14.4 kW
#Modules (1-axis)	-	168	1155	176	40	48	50	120
#Modules (Lat. Tilt)	216	-	-	-	-	-	-	-
#Modules (String)	3	21	21	8	8	8	12	23
String Voltage (Voc)	65	455	455	505	505	485	532	483
Years Fielded	18	13.3	13.3	11.7	3-4	11.7	11.7	11.7
Structure	Framed	Framed	Frameless	Framed	Framed	Framed	Framed	Framed



Figure 5: Pictures of all models in APS-STAR power plant

All these modules, shown in Table 1 (except A18 modules) are to be statistically analyzed to identify the performance parameter causing power degradation. This part of the project required the process of statistical hypothesis testing using Minitab software.

### **3.4 Statistical Hypothesis Testing using Minitab Software**

The use of statistics to determine the chances for a given condition to be rejected or not rejected is called hypothesis testing. The following are the steps involved in hypothesis testing using Minitab software.

- 1) Firstly, the null hypothesis and alternative hypothesis need to be clearly defined. Null hypothesis can be defined as a general condition and is denoted as  $H_0$ . When the hypothesis does not satisfy the null hypothesis, it is called as Alternative hypothesis and is denoted as  $H_1$ . The alternative hypothesis becomes true only when the probability does not exceed the identified significance level (in this case  $\alpha=0.05$ ). The null hypothesis can be mathematically defined as,  $H_0: \mu_0=\mu_1$ , where:  $\mu_0$ ,  $\mu_1$  are mean of population 1 and 2 respectively. Whereas, the mathematical definition for alternative hypothesis can be written as  $H_1: \mu_0>\mu_1$  or  $\mu_0<\mu_1$  or  $\mu_0\neq\mu_1$ .
- 2) The degradation per year values for short-circuit current, open circuit voltage and fill factor are copied into the Minitab worksheet. A two sample t test is performed upon the selected columns. Columns like degradation for  $I_{sc}$  with degradation for fill factor and degradation for  $I_{sc}$  with degradation for  $V_{oc}$  are compared. The options button in the 2 sample t test dialog box consists of various comparison symbols and usually  $<$  or  $>$  symbols are chosen for comparison.
- 3) Once the test has been performed, a working window pops up with various numeric values such as test statistic value and the probability value. The probability value obtained should be compared with the significance level (i.e.  $\alpha=0.05$ ). If the P value is smaller than that of significance value, the alternative hypothesis becomes true and the null hypothesis can be rejected. By this statistical approach the parameter affecting the

power drop could be found. An example of hypothesis testing has been demonstrated in appendix K.

A graphical method to find the factor affecting power drop is achieved by plotting graphs with power drop (on the X-axis) and other parameters like short circuit current, open circuit voltage and fill factor ( on the Y-axis). The graph showing a linear increase will be the factor affecting the power drop. Statistical approach is a scientific and reliable approach to identify the parameters(s) influencing power loss. The plots for graphical methods for all the models are provided in the appendix section I.

## Chapter 4

### 4. RESULTS AND DISCUSSION

#### 4.1 Relative $I_{sc}$ with diffused component and cosine effects

When the ratio of direct normal irradiance ( $G_{dni}$ ) to global irradiance was 87%, the first set of data was collected. For each angle of incidence, the  $I_{sc}$  data was measured and collected. Figure 5 shows the relative  $I_{sc}$  which contains both the diffused components and the cosine effects. The plot obtained shows that the data is identical for all the 5 type of technologies. The true  $I_{sc}$  value obtained (relative optical response) is free from diffused component and the cosine effect. Hence the  $I_{sc}$  data shown in the Figure 6 has to be corrected.

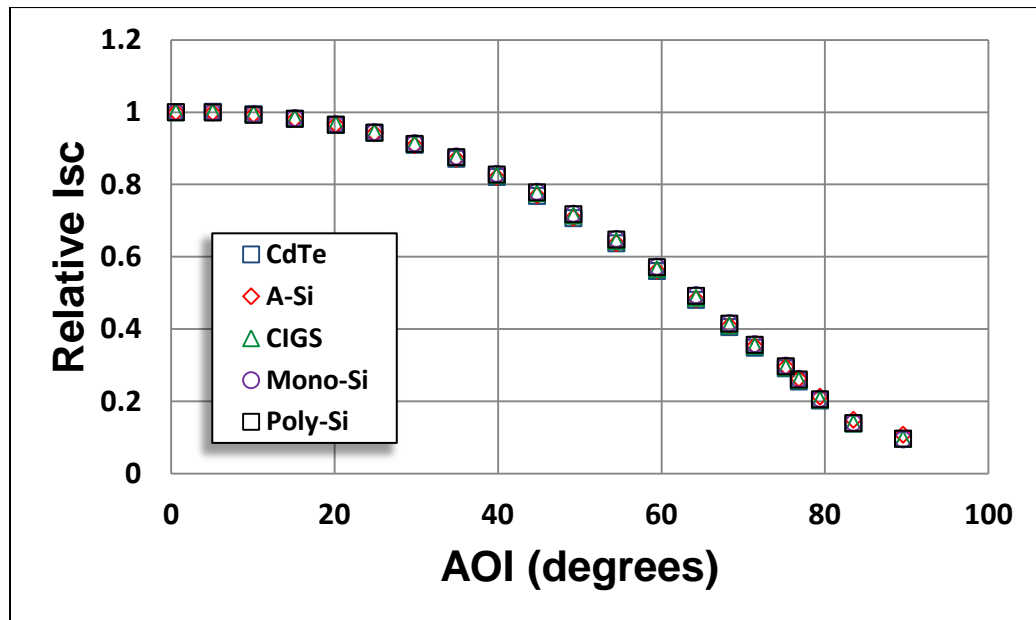


Figure 6: Relative  $I_{sc}$  with diffused component and cosine effects

#### 4.2 Relative $I_{sc}$ without diffused component and cosine effects

According to the requirements of the standard, the diffused component of incident light should not be greater than 10% of the total irradiance during the experiment. In order to remove the influence of diffused component, the data should be corrected. This can be done either by

using the reference cell method or the pyranometer/pyrheliometer method as prescribed by the standard. In the reference cell method, the procedure describes: *“If the diffused component exceeds 10%, it can be subtracted after measuring the angular response with blocked direct light component or the diffuse component can be blocked to below 10% by reducing the field of view of the diffuse component, for example by collimating the incident light reaching the test module.”*

The  $I_{sc}$  obtained from this method does not contain any diffused component as it is subtracted from the global irradiance.. The  $I_{sc}(\theta)$  can be directly used in equation 3 to obtain the relative optical response which does not include the diffused component and the cosine effects.

In the pyranometer/pyrheliometer method, two procedures were evaluated: IEC procedure (as described in chapter 3); Sandia procedure. The Sandia procedure uses the following formulae and is also been described in the appendix A . The relative optical response,  $f_2(AOI)$ , is given as

$$f_2(AOI) = \frac{\left[ E_o \left( \frac{I_{sc}}{(1 + \alpha_{isc}(T_c - 25)) \cdot I_{scr}} \right) - (E_{poa} - E_{dni} \cdot \cos(AOI)) \right]}{[E_{dni} \cdot \cos(AOI)]} \quad (4)$$

$$I_{scr} = I_{sc} * \left( \frac{E_o}{E_{poa}} \right) * (1 + \alpha_{isc}(T_c - 25)) \quad (5)$$

Where:

$E_{dni}$  = Direct normal solar irradiance ( $W/m^2$ )

$E_{poa}$  = Global solar irradiance on the plane-of-array (module)( $W/m^2$ )

$E_o$  = Reference global solar irradiance, typically  $1000 W/m^2$

$AOI$  = Angle between solar beam and module normal vector (deg)

$T_c$  = Measured module temperature ( $^{\circ}C$ )

$\alpha_{isc}$  = Short-circuit current temperature coefficient ( $1/^{\circ}C$ )

$I_{scr}$  = Module short circuit current at STC conditions (A)

$I_{sc}$  = Measured short circuit current (A)

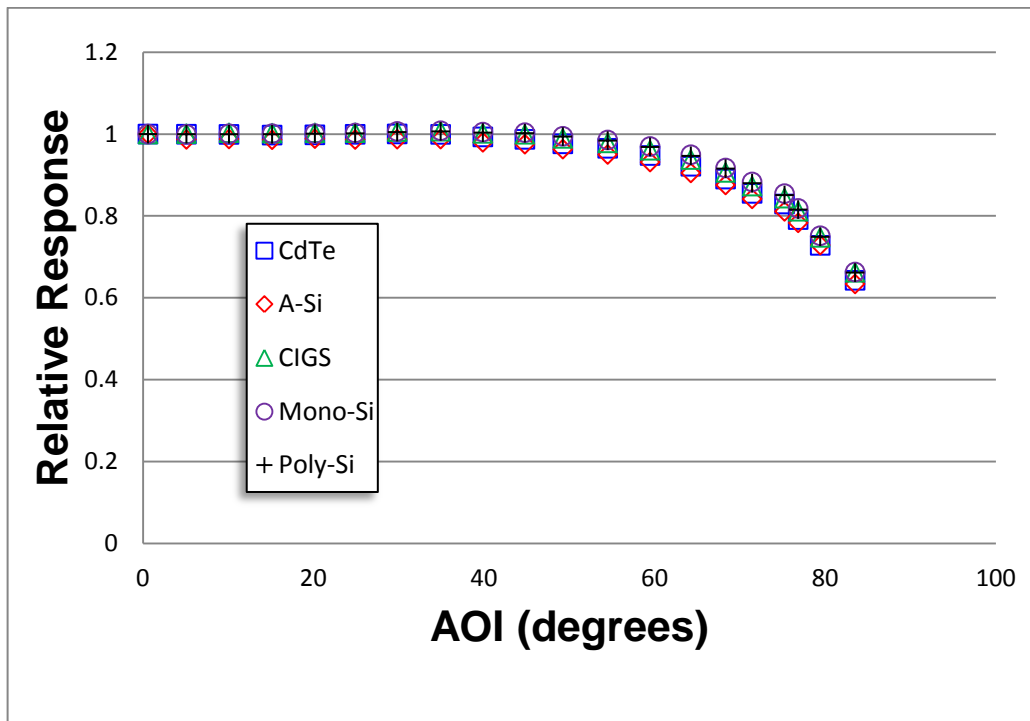


Figure 7: Relative  $I_{sc}$  without diffused component and cosine effects – IEC method

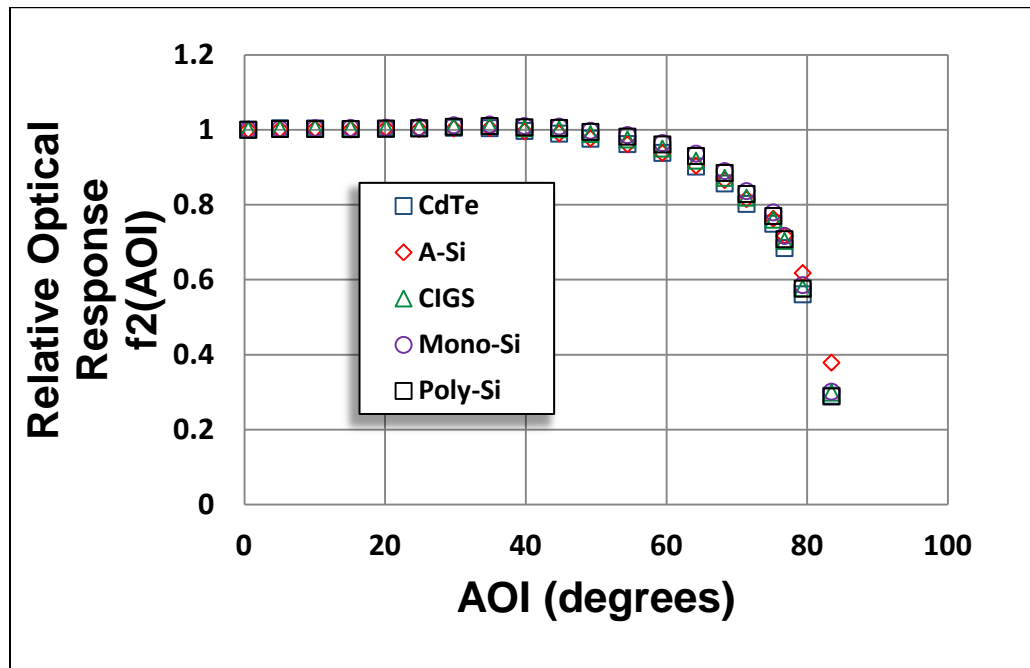


Figure 8: Relative  $I_{sc}$  without diffused component and cosine effects – Sandia method

The plots obtained from IEC procedure (equations 1, 2 & 3) and Sandia procedure (equation 4 & 5) are shown in Figures 7 & 8, respectively. Both these procedure have similar results. Figure 9 shows the data can be influenced at higher values of AOI ( $>60^\circ$ ) by the type of pyranometer due to the sensitivity of AOI on the calibration factors of the pyranometers above  $60^\circ$ .

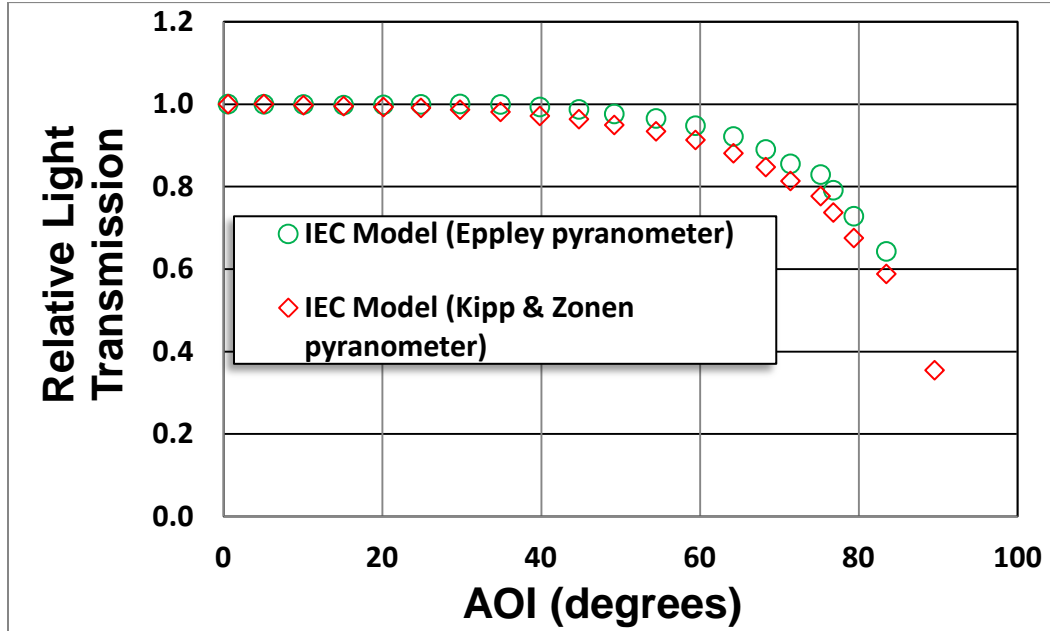


Figure 9: Comparison between Eppley and Kipp & Zonen pyranometers – CdTe Module

In both the reference cell and pyranometer/pyrheliometer method, there are pros and cons. With the reference cell method, there is no spectral mismatch error (if the test is long) between the reference cell and the test module when a matching reference cell technology is used. However it requires additional module measurements with collimated lights or blocked lights. In the pyranometer/pyrheliometer method, extra module measurements are not required. But, there is spectral mismatch error between the test modules, pyranometer and pyrheliometer, if the air mass exceeds 1.5. This error can be considered of second order issue with no impact on the final data if the experiment is of short duration.



### 4.3 Comparison between the models

The data obtained from  $f_2$  (AOI) for the modules with glass superstrate, Sandia National Laboratories found a generic polynomial model as shown in equation 6 (see Appendix A for details)

$$f_2(\text{AOI}) = 1 - 2.4377\text{E-}3(\text{AOI}) + 3.1032\text{E-}4(\text{AOI})^2 - 1.2458\text{E-}5(\text{AOI})^3 + 2.1122\text{E-}7(\text{AOI})^4 - 1.3593\text{E-}9(\text{AOI})^5 \quad (6)$$

Many theoretical AOI models have been developed for the air-glass interface. The data obtained from Sandia model and the IEC model for a glass superstrate (say CdTe) is compared with the generic polynomial model of Sandia and Martin and Ruiz AOI model for air-glass interface. All the plots are found to be identical with each other confirming that the relative optical response is dictated by the air-glass interface. The draft standard states: *“For modules with a flat uncoated front glass plate made of standard solar glass, the relative light transmission into the module is primarily influenced by the first glass-air interface. In this case, the test does not need to be performed; rather, the data of a flat glass air interface can be used.”* The experimental data and the theoretical model confirm and validate the above statement.

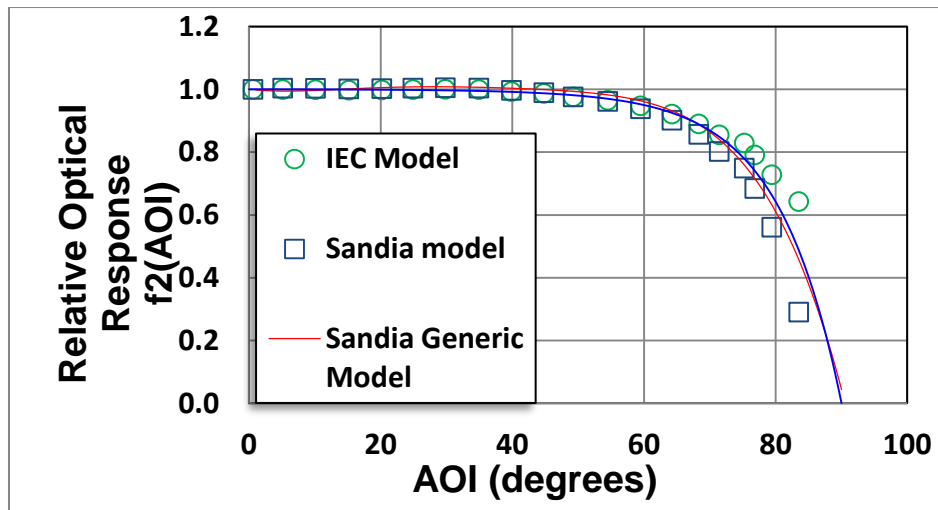


Figure 10: Comparison between various models developed by different institutions

To obtain accurate results, as in the case of non-glass (including AR coated glass) or non-planar (non-flat) glass superstrate modules, the approach suggested by Sandia National Laboratories may be followed (see appendix A). The results are similar for flat air-glass interface modules, the reference module (flat glass with matched cell technology) and the module under test can be analyzed and experimented simultaneously to remove any data processing errors.

#### 4.4 Uncertainty Analysis

Precautions were taken to increase the accuracy of the procedure and test setup. For equations 4 and 5, each uncertainty contributor was taken into account and the magnitude of associated uncertainty was assigned based on the calibration report specifications. The table for uncertainties is given below in Table 2.

Table 2: Uncertainty of various uncertainty contributors in equations 4 and 5

Uncertainty Contributor (Ui)	Uncertainty
Isc (Uisc)	1.000%
Global Irradiance (Uepoa)	1.400%
Temperature Coefficient (Ualpha)	0.010%
Module Temperature (Ut)	0.75%
Direct Irradiance (Udni)	1.100%
Angle of Incidence (UAOI)	1.0%

The uncertainty for  $f_2$  (AOI) was taken as the square root of the sum of squares of the estimates of uncertainty times the squares of the corresponding coefficients of sensitivity. By taking the derivative of  $f_2$  (AOI) equation with respect to the uncertainty contributor, the sensitivity coefficients can be found.

$$u_c = \sqrt{\sum_i c_i^2 u_i^2} \quad (7)$$

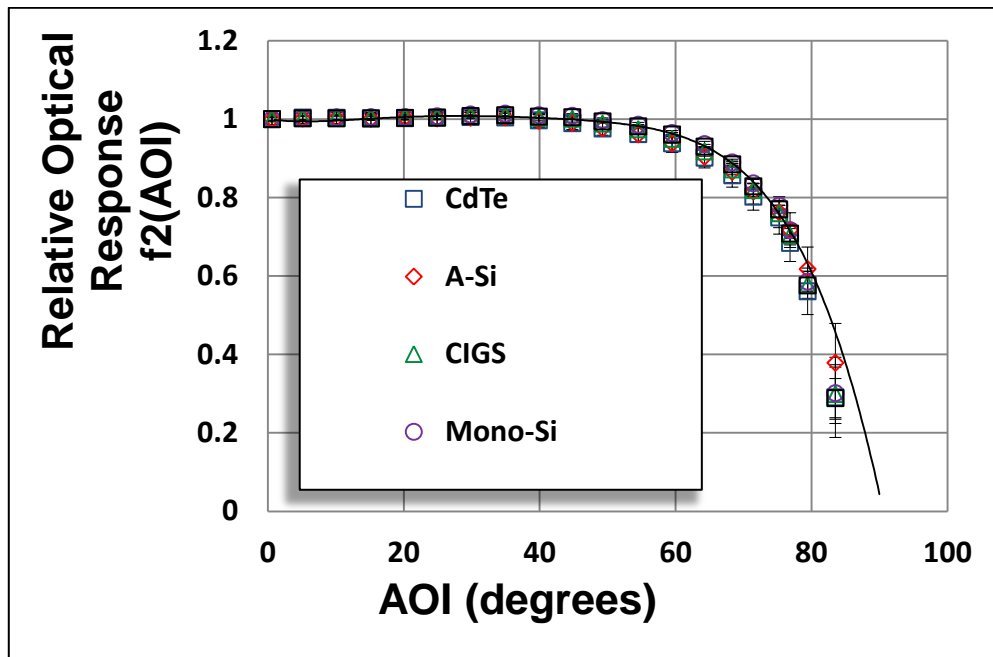


Figure 11: Uncertainties obtained as error bars presented for all modules

#### 4.5 Results and Discussions for Power Plant Analysis

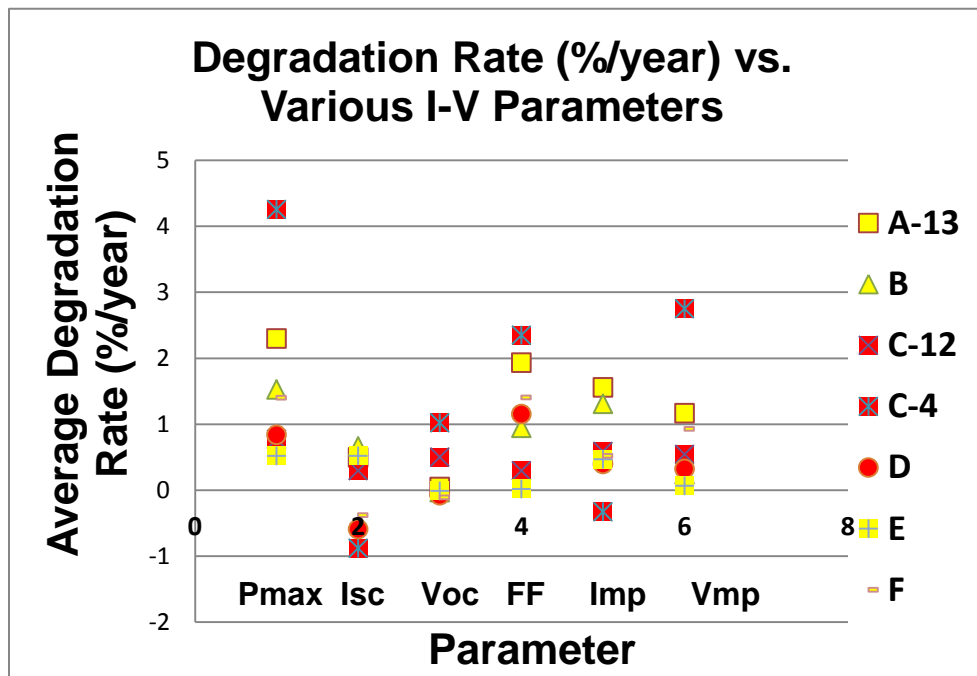


Figure 12: Plot for I-V Parameters versus average annual degradation rates for all models

The uncertainties obtained are presented as error bars in Figure 10 for all types of module technologies. The uncertainty of  $f_2(\text{AOI})$  increases with increasing AOI. For this experiment, a single sensitivity factor for the pyranometers for all values of AOI was used. But still the sensitivity increases slightly with AOI going beyond  $60^\circ$ . Therefore the uncertainty increases with increasing AOI. From the data collected by the previous researcher, the above plot has been constructed. The annual mean and median degradation rates for each model are included in the appendix.

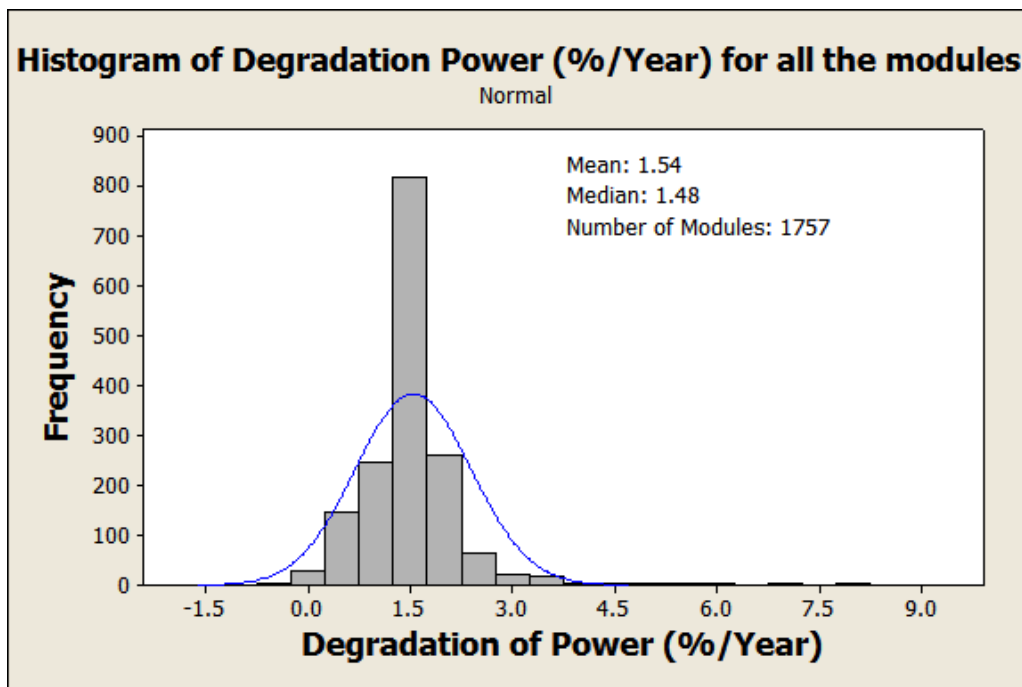


Figure 13: Histogram of degradation rates

The histogram for all the modules analyzed is given below with a distribution fit. The histogram in figure 13 shows a mean and median degradation rates for 1757 modules, except the A18 fixed tilt modules, which were not considered for the entire analysis. It shows a median degradation rate of 1.48% per year. The histogram also indicates the modules are degrading with a mean of 1.54% per year.

Table 3: Values for mean and median for each model

Model	Degradation of Power (%/Year)	
	Mean	Median
A13	2.27	2.20
B	1.53	1.51
C12	0.77	0.59
C4	4.25	4.76
D	0.84	0.50
E	0.52	0.55
F	1.40	1.29

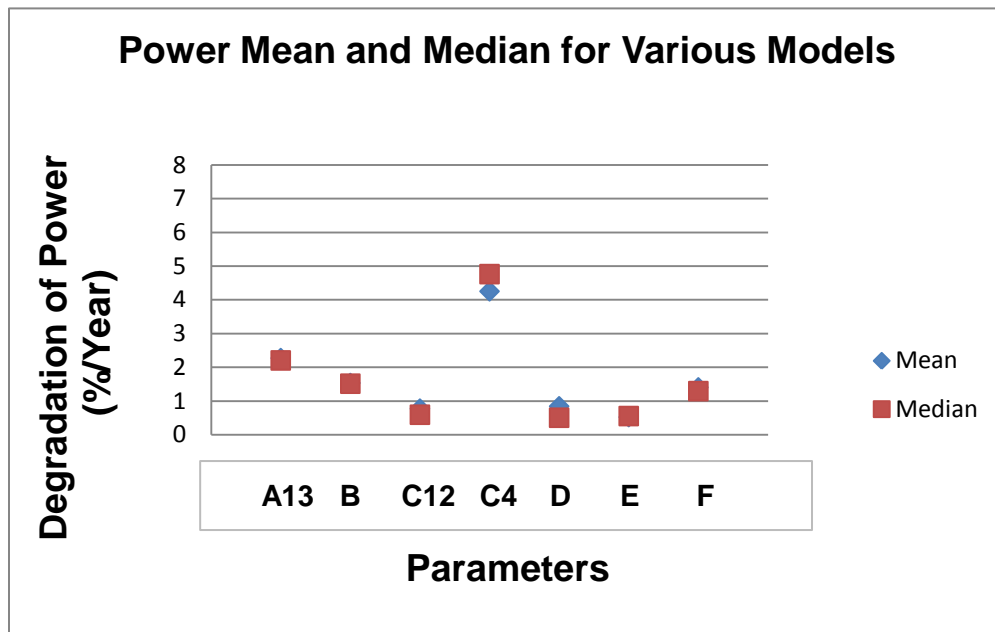


Figure 14: Power Mean and Median for various models

The mean and median of these modules should be compared to determine the degradation rate per year of all modules in a particular model is at a same rate. The histogram for degradation of power for each model is shown in appendix J. The table 3 shows the mean and median values for all the models. The mean and median data are closely matching and it

indicates that the data is not significantly skewed. The plots for mean and median for all models are shown below in Figure 15 through Figure 21.

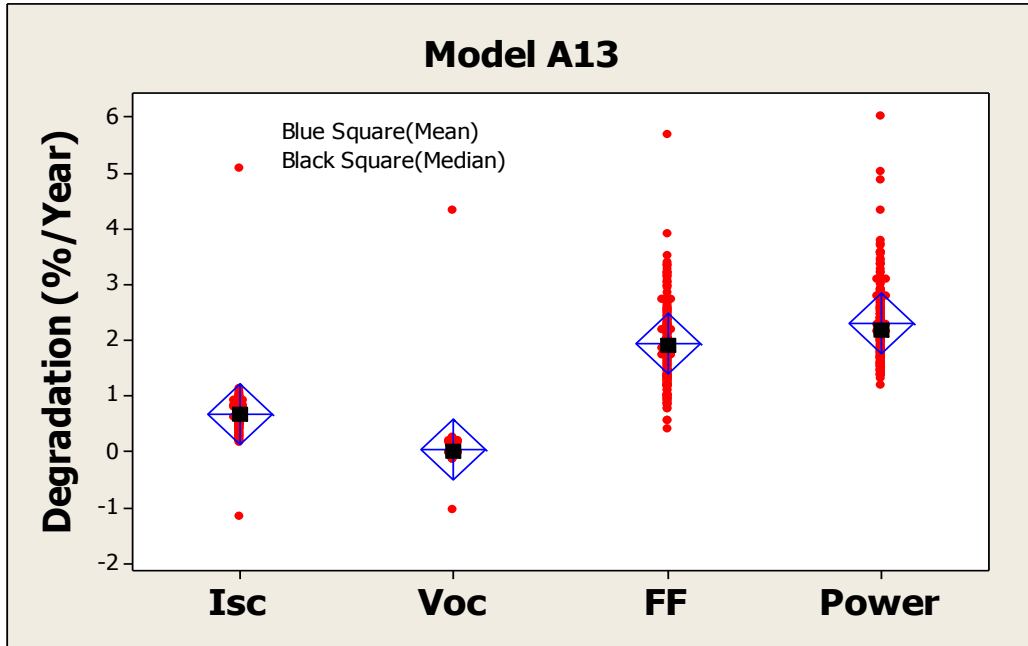


Figure 15: Plot for various I-V parameter degradation (%/year) for Model A13

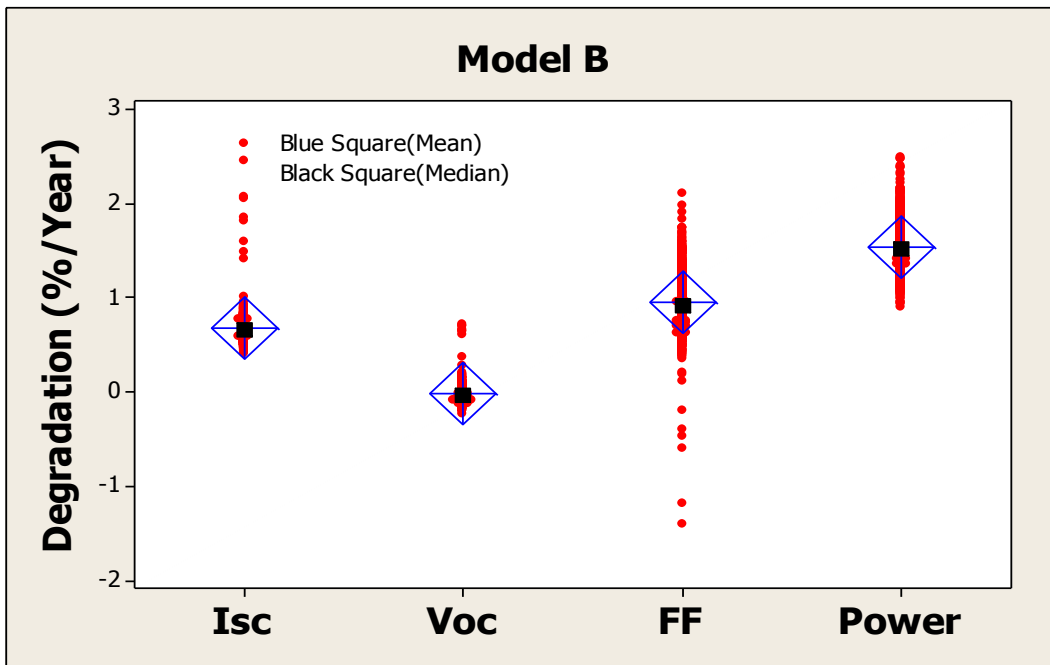


Figure 16: Plot for various I-V parameter degradation (%/year) for Model B

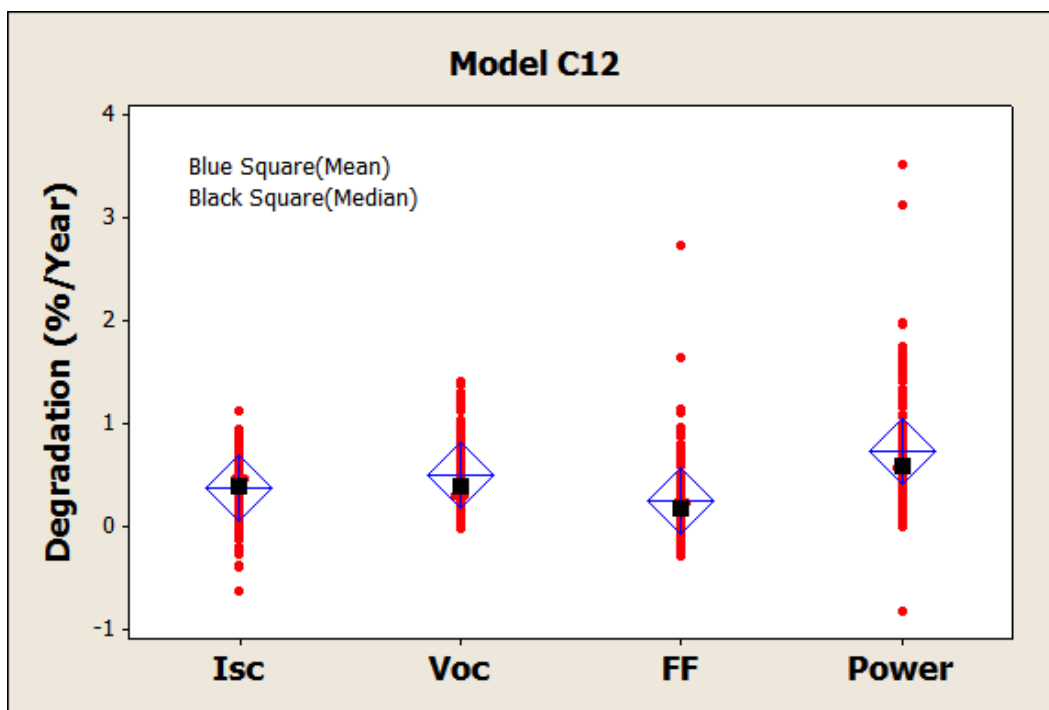


Figure 17: Plot for various I-V parameter degradation (%/year) for Model C12

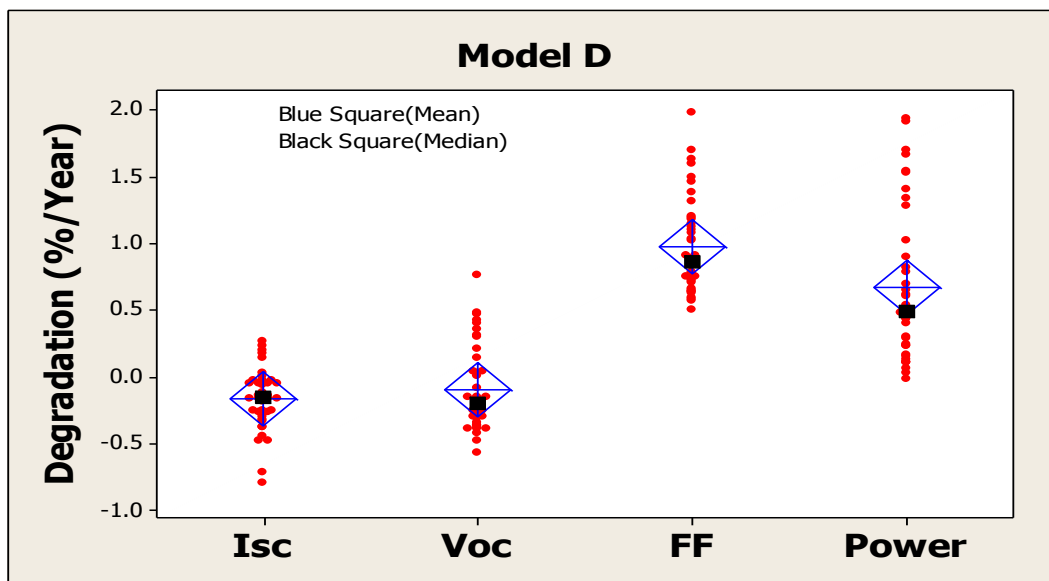


Figure 18: Plot for various I-V parameter degradation (%/year) for Model D

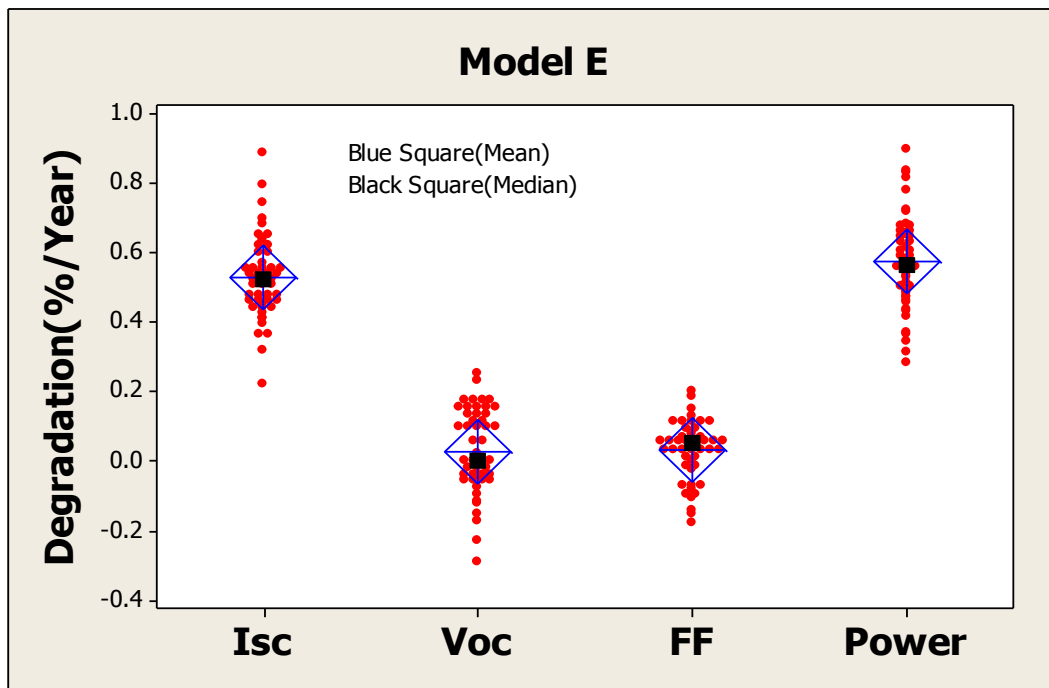


Figure 19: Plot for various I-V parameter degradation (%/year) for Model E

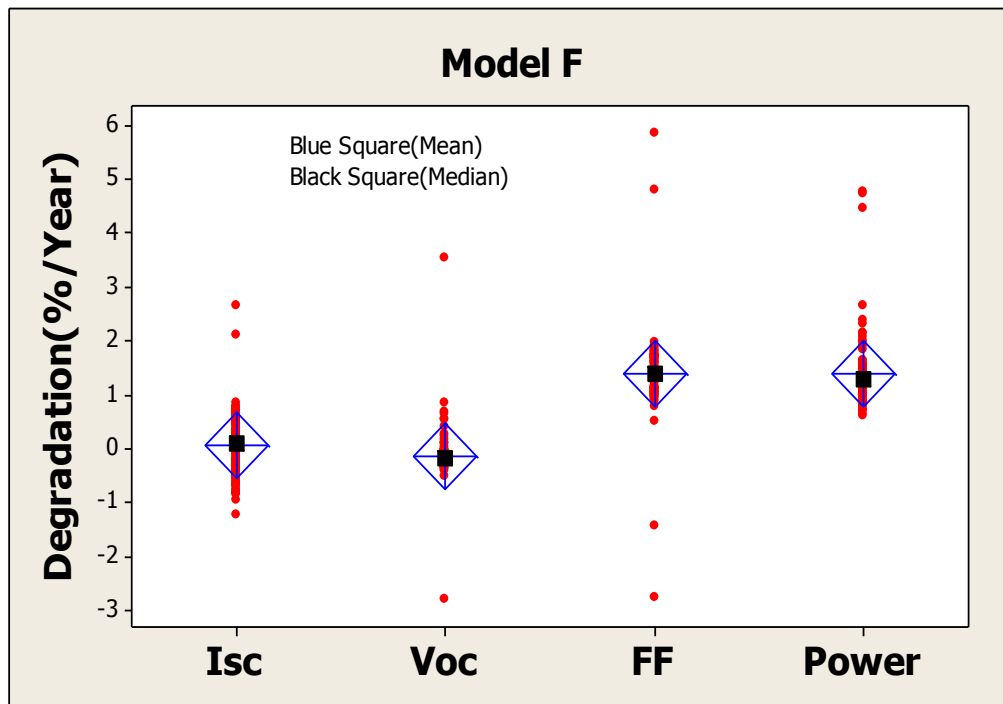


Figure 20: Plot for various I-V parameter degradation (%/year) for Model F



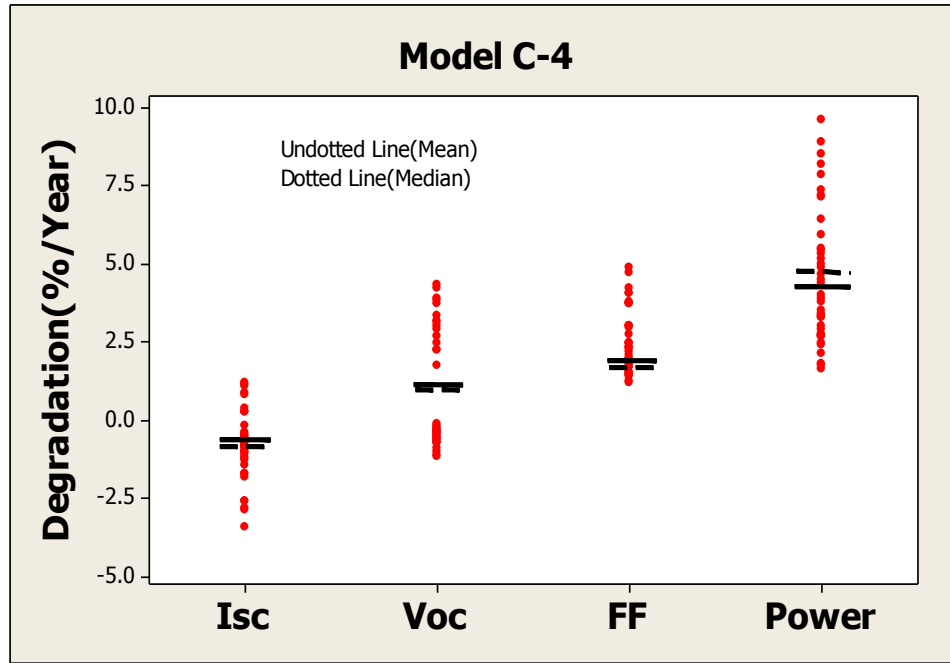


Figure 21: Plot for various I-V parameter degradation (%/year) for Model C4

Table 4: Primary parameter and the primary visual defect causing the degradation in power for each model

Model [Years]	Average $P_{max}$ Degradation (%/Year)	Order of Statistical Parameters Affected	Order of Statistical Visual Defects	Potential Primary Reasons for $P_{max}$ Degradation
A13 [13] (glass/polymer)	2.29	$FF \gg I_{sc} > V_{oc}$	DE, SD	Series resistance increase(SBD) DE
B [12] (glass/polymer)	1.53	$FF \gg I_{sc} > V_{oc}$	DE, MSW	Series resistance increase (SBD), DE
C12 [12] (glass/glass)	0.77	$V_{oc} > I_{sc} = FF$	DLM, BC, HS	DLM
C4 [4] (glass/glass)	4.14	$FF > V_{oc} \gg I_{sc}$	BC, DLM, HS	Unknown
D [12] (glass/polymer)	0.83	$FF \gg I_{sc} = V_{oc}$	DE	Series resistance increase(SBD)
E [12] (glass/polymer)	0.57	$I_{sc} \gg FF = V_{oc}$	MSW	MSW
F [12] (glass/polymer)	1.40	$FF \gg I_{sc} = V_{oc}$	MD, SD	Series resistance increase (SBD)

From the table and graphs above we clearly see that all mean and median are nearly equal for all modules of a particular model.

The table below shows the primary factor and major visual defect that is causing the drop in power for modules of each model. The abbreviations of the defects found statistically are as follows: Discoloration of Encapsulant (DE), Seal Deterioration (SD), Minor Substrate Warping (MSW), Delamination (DLM), Broken Cells (BC), Hotspots (HS), Metallization Discoloration (MD), and Solder Bond Deterioration (SBD).

The primary visual defects are shown on a Pareto charts for each model in Appendix H.

## Chapter 5

### 5. CONCLUSIONS

Validation of standard IEC 61853-2 (draft) for measuring the effect of AOI on PV modules was accomplished using outdoor test method for five different technologies. The important results obtained are:

- With glass as superstrate for all five different technologies tested, the relative light transmission plots are practically the same. The air-glass interface of the PV modules primarily governs reflective losses as demonstrated with the theoretical curves obtained at the air-glass interface.
- Models developed by Sandia National Laboratories and the theoretical air-glass interface models for glass superstrate matched with the relative transmission plots that was obtained using the IEC 61853-2 model.
- The analysis and conclusion of this study confirms and validates the statement “*for the flat glass superstrate modules, the AOI test does not need to be performed; rather, the data of a flat glass air interface can be used.*” delineated in the IEC 61853-2 standard is accurate.
- In order to test a non-glass or non-planar module and get an accurate result, the reference module (flat glass superstrates and matched cell technology) approach can be done in accordance with the procedure described by Sandia National Laboratories.

The important conclusions obtained from the power plant study were:

- Significant number of modules falls close to the mean value (as indicated by the median value) of degradation rate but a few modules have high degradation rates. This indicates that the string power could be lower from that of the sum of individual power of the modules in that string.

- The primary causes for power degradation in all glass/polymer modules appear to be due to the fill factor loss and short circuit current loss. The primary degradation modes attributed to these losses are solder bond deterioration and encapsulant discoloration.
- Power degradation in modules with glass/glass construction appears to be due to a loss in open circuit voltage. The primary degradation mode attributed to the voltage loss is encapsulant delamination.

## REFERENCES

- [1] IEC 61853-2 (Draft), *Photovoltaic (PV) Module Performance Testing and Energy Rating - Part 2: Spectral Response, Incidence Angle and Module Operating Temperature Measurements*, May 2012.
- [2] King, D.L., Kratochvil, J. A., Boyson, W.E., *Measuring solar spectral and angle-of-incidence effects on photovoltaic modules and solar irradiance sensors*, IEEE Photovoltaic Specialists Conference, Anaheim, California, 1997.
- [3] King, D.L., *Measuring Angle of Incidence (AOI) Influence on PV Module Performance*", Private Communication, June 2012 (this document is reproduced in the Appendix of this report)
- [4] Martin, N., and J. M. Ruiz, J.M., *Annual Angular Reflection Losses in PV Modules*, Progress in Photovoltaics, 13, 75–84, 2005.
- [5] Soto, W.D., Klein, S. A., Beckman, W.A., *Improvement and validation of a model for photovoltaic array performance*, Solar Energy, 80, 78–88, 2006.
- [6] Sjerps-Koomen, E.A., Alsema, E.A., Turkenburg, W.C., *A Simple model for PV module reflection losses under field conditions*, Solar Energy, 57, 421-432, 1997.
- [7] Singh, J., *Investigation of 1,900 Individual Field Aged Photovoltaic Modules for Potential Induced Degradation (PID) in a Positive Biased Power Plant* (Master's Thesis), Arizona State University, AZ
- [8] D.C. Jordan et al., *PV Degradation Risk*, World Renewable Energy Forum, Denver, CO, USA, May 2012.
- [9] Jordan, D.C., Kurtz, S.R., *Photovoltaic Degradation Rates – an Analytical Review*, Progress in Photovoltaics: Res. Appl., October 2011
- [10] Smith, R.M., Jordan, D.C., Kurtz, S.R., *Outdoor PV Module Degradation of Current-Voltage Parameters*, World Renewable Energy Forum, Denver, CO, USA, May 2012
- [11] Jordan, D.C., Wohlgemuth, J.H., Kurtz, S.R., *Technology and Climate Trends in PV Module Degradation*, 27<sup>th</sup> European Photovoltaic Solar Energy Conference and Exhibition, Frankfurt, Germany, 2012
- [12] Reis, A.M., Coleman N.T., Marshall M.W., Lehman P.A., Chamberlin, C.E., *Comparison of PV module performance before and after 11-years of field exposure*, IEEE PV Specialists Conference, New Orleans, LA, USA, 1432–1435 (2002)
- [13] Chamberlin, C.E., Rocheleau, M.A., Marshall, M.W., Reis, A.M., Coleman, N.T., Lehman, P.A., *Comparison of PV Module Performance Before and after 11 and 20 Years of Field Exposure*, IEEE PV Specialists Conference, Seattle, WA, USA, (2011)

## **APPENDIX A**

SANDIA PROCEDURE TO DETERMINE RELATIVE OPTICAL RESPONSE  $f_2(\text{AOI})$

## Measuring Angle-of-Incidence (AOI) Influence on PV Module Performance

David L. King (June 2012)

Private Communication

There are two AOI influences that need to be considered, one is “mechanical” and the other is “optical.” The mechanical influence really doesn’t have anything to do with the module itself, but rather its orientation relative to the incident sunlight, often called the “cosine effect.” The beam solar irradiance incident on the module is reduced by  $\cos(\text{AOI})$ . The optical effect is due to the surface characteristics of the module, which can be highly planar (float glass), dimpled (rolled glass), coated with anti-reflection (AR) coatings, heavily textured for light gathering at large AOI, or specifically patterned for optical concentration purposes. The primary influence on the optical effect is increasing reflectance loss as AOI increases. Both of these AOI influences apply primarily to the beam or direct component of sunlight, rather than the diffuse component of sunlight. The Sandia module performance model attempts to account for both these influences using an expanded expression for the solar irradiance, called the effective solar irradiance ( $E_e$ ), which in turn determines the module’s short-circuit current ( $I_{sc}$ ). Equation (A1) gives the Sandia expression for  $E_e$ , and Equation (A2) gives the resulting equation for  $I_{sc}$ . The intent of this document is to provide a discussion of the procedures that can be used to empirically measure the optical effect,  $f_2(\text{AOI})$ .

$$E_e = [E_{dni} \cdot \cos(\text{AOI}) \cdot f_2(\text{AOI}) + f_d \cdot (E_{poa} - E_{dni} \cdot \cos(\text{AOI}))] / E_o \quad (\text{A1})$$

$$I_{sc} = I_{sc0} \cdot [1 + \alpha_{Isc} \cdot (T_c - 25)] \cdot f_1(\text{AM}_a) \cdot E_e \quad (\text{A2})$$

Where:

$E_e$  = Solar irradiance actually captured and used by module (dim or suns)

$E_{dni}$  = Direct normal solar irradiance ( $\text{W/m}^2$ )

$E_{poa}$  = Global solar irradiance in the plane-of-array (module) ( $\text{W/m}^2$ )

$E_o$  = Reference global solar irradiance, typically  $1000 \text{ W/m}^2$

$f_d$  = Fraction of diffuse irradiance used by module, typically

assumed = 1 (dim)

AOI = Angle between solar beam and module normal vector (deg)

$T_c$  = Measured module (cell) temperature ( $^{\circ}\text{C}$ )

$\alpha_{sc}$  = Short-circuit current temperature coefficient ( $1/^{\circ}\text{C}$ )

$f_1(\text{AM}_a)$  = Empirical relationship for solar spectral influence on  $I_{sc}$

versus air mass

$I_{sc0}$  = Module short-circuit current at STC conditions (A)

$I_{sc}$  = Measured short-circuit current (A)

#### Direct Measurement of $f_2(\text{AOI})$

The direct procedure for measuring  $f_2(\text{AOI})$  involves measuring module  $I_{sc}$  as the module is moved in angular increments using a solar tracker through a wide range of AOI conditions, 0 deg to 90 deg. The challenge is to conduct the test in a way that either minimizes or compensates for all the factors in Equations (A1) and (A2) that influence the measured  $I_{sc}$  values. The following bullets identify desirable conditions and approaches, depending on the capabilities of the test equipment available.

- Conduct test during clear sky conditions when the direct normal irradiance is the dominant component, e.g. when the ratio of direct normal divided by global normal irradiance is greater than about 0.85. This reduces the influence of diffuse irradiance on the determination of  $f_2(\text{AOI})$ .
- Conducting the test near solar noon also has a couple advantages, variation in the solar spectrum during the test is minimized, and the full range for AOI can typically be achieved by changing only the elevation angle of a two-axis solar tracker.
- Measure  $I_{sc}$ ,  $E_{dni}$ ,  $E_{poa}$ , and  $T_c$  associated with each AOI increment.  $E_{dni}$  should be measured with a thermopile pyrheliometer, and  $E_{poa}$  should ideally be measured using a thermopile pyranometer that has been calibrated as a function of AOI.



- Module temperature will vary during the test, so measured temperature should be used to translate measured  $I_{sc}$  values to a common temperature, e.g. 25°C.
- If possible, record data over the full range of AOI as rapidly as possible, so that solar spectral variation can be ignored, less than 30-min test period is desirable. If the test period must be longer, then a spectral correction to measured  $I_{sc}$  can be done using a previously determined  $f_1(AM_a)$  relationship.

The Sandia model equations (A1) and (A2) can be solved to provide an equation for the angle-of-incidence relationship,  $f_2(AOI)$ , as a function of the measured variables, Equation (A3).

$$f_2(AOI) = \{ [I_{sc} * E_o / (I_{sco} * f_1(AM_a) * (1 + \alpha_{isc}(T_c - 25)))] - f_d * (E_{poa} - E_{dni} * \cos(AOI)) \} / (E_{dni} * \cos(AOI)) \quad (A3)$$

In order to simplify, recognize that by definition  $f_2(AOI)=1$  when  $AOI=0$  degrees.

Therefore, Equation (A3) can be solved for the  $I_{sco}$  value at the start and end of the outdoor test period when  $AOI=0$  degrees. The value solved for is not exactly  $I_{sco}$  at STC because the air mass value may not be exactly  $AM_a=1.5$  at the time of day when the  $AOI=0$  deg conditions were achieved. This calculated value is only intended to provide a reference value for short-circuit current in order to normalize  $f_2(AOI)=1$  when  $AOI=0$  deg, so to avoid confusion call the calculated value  $I_{scr}$ .

$$I_{scr} = I_{sc} * E_o / \{ f_1(AM_a) * (1 + \alpha_{isc}(T_c - 25)) * (E_{dni} + f_d * (E_{poa} - E_{dni})) \} \quad (A4)$$

After determining the value for  $I_{scr}$  using the average value for several measurements when  $AOI=0$  deg, the measured values for  $f_2(AOI)$  can be determined using Equation (3), by substituting the  $I_{scr}$  value for  $I_{sco}$ .

Further simplification in the determination of  $f_2(AOI)$  can be made for conventional flat-plate modules, depending on the test procedure and assumptions made. If data for the full range of AOI is recorded in a relatively short period of time, then the influence of varying solar spectrum is likely to be negligible. In addition, for conventional flat-plate modules the assumption is usually

made that they capture both diffuse and direct irradiance; therefore  $f_d=1$ . Under these simplified conditions, Equations (A3) and (A4) can be rewritten as Equations (A5) and (A6).

$$I_{scr} = I_{sc} * (E_o/E_{poa}) * (1 + \alpha_{isc}(T_c - 25)) \quad (A5)$$

$$f_2(AOI) = [E_o * (I_{sc}/(1 + \alpha_{isc}(T_c - 25)))/I_{scr} - (E_{poa} - E_{dni} * \cos(AOI))]/(E_{dni} * \cos(AOI)) \quad (A6)$$

For conventional flat-plate glass modules, this procedure should result in empirical  $f_2(AOI)$  relationships similar to those shown in Figure A1. As previously mentioned, AR-coated glass or heavily textured glass will provide different results. For the simple case with a planar glass surface, Snell's and Bouguer's optic laws along with glass optical properties (index of refraction, extinction coefficient, thickness) can also be used to calculate a theoretical relationship for  $f_2(AOI)$ , as done by DeSoto in Reference [1].

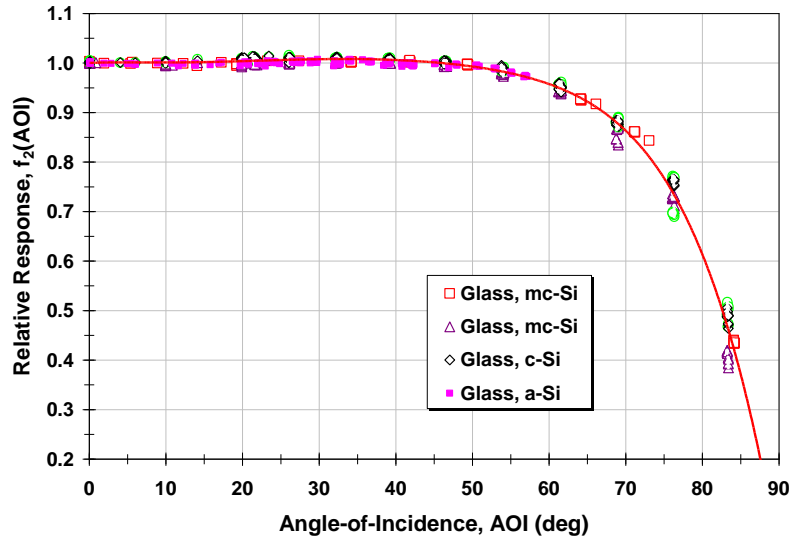


Figure A 1: Empirical  $f_2(AOI)$  measurements by Sandia National Laboratories for conventional flat-plate modules with a planar glass front surfaces.

Although polynomial fits to measured data can be problematic, ten years ago when the procedure was developed and the Sandia module database initiated, a fifth order fit was used to represent the measured data and reduce measured data problems. The “generic” polynomial used for the majority of typical glass-surface modules is given below.

$$f_2(\text{AOI}) = 1 - 2.4377\text{E-}3(\text{AOI}) + 3.1032\text{E-}4(\text{AOI})^2 - 1.2458\text{E-}5(\text{AOI})^3 + 2.1122\text{E-}7(\text{AOI})^4 - 1.3593\text{E-}9(\text{AOI})^5$$

#### Relative (Comparison) Measurements for $f_2(\text{AOI})$

Although not presented in this document, an alternative test procedure providing simultaneous measurements of the  $I_{sc}$  of a test module and a reference module may possibly provide a more accurate and repeatable process. The reference module is assumed to have “known  $f_2(\text{AOI})$ ” characteristics. The reference device could be a module or an individual reference cell, ideally with matching cell technology to provide equivalent solar spectral sensitivity. For a reference device with ideally planar glass surface, the “known  $f_2(\text{AOI})$ ” could be derived from optical laws, perhaps providing a more fundamental basis for the outdoor test procedure.

#### References

- [1] W. DeSoto, S.A. Klein, W.A. Beckman, “Improvement and Validation of a Model for Photovoltaic Array Performance,” Solar Energy, August 2005.

## **APPENDIX B**

### **CROSSCHECKING OF AOI DEVICE USING MANUAL METHOD**

In this study, the AOI was directly determined using an AOI device purchased from MicroStrain. However, in the absence of this device, the AOI value can also be determined using a manual calculation (equation B1) given by Sandia National Laboratories<sup>2</sup>.

$$AOI = \cos^{-1}(\cos(T_m) \cos(Z_s) + \sin(T_m) \sin(Z_s) \cos(AZ_s - AZ_m)) \quad (B1)$$

Where:

AOI = solar angle of incidence (degrees)

$T_m$  = tilt angle of module (degrees, 0° is horizontal)

$Z_s$  = zenith angle of the sun (degrees)

$AZ_m$  = azimuth angle of module (0°=North, 90°=East)

$AZ_s$  = azimuth angle of sun (degrees)

As shown in Figure B1 (azimuth rotation) and Figure 1B (elevation rotation) below, the accuracy of the AOI device used in this project was crosschecked with the manual method using equation 1 given above. These plots confirm that the AOI data obtained using the MicroStrain device was reliable and accurate. For azimuth angle, the tracker was allowed to rotate to its full Westward rotation angle and tracked azimuthally to the East. The azimuth angle of the module was manually measured by dividing the diameter of the tracker pole into 360° and fixing a dial to the rotating head of the tracker to indicate its change in angle. Since the azimuthal rotation of the tracker was limited, azimuth verification could only be obtained for AOI up to 63°.

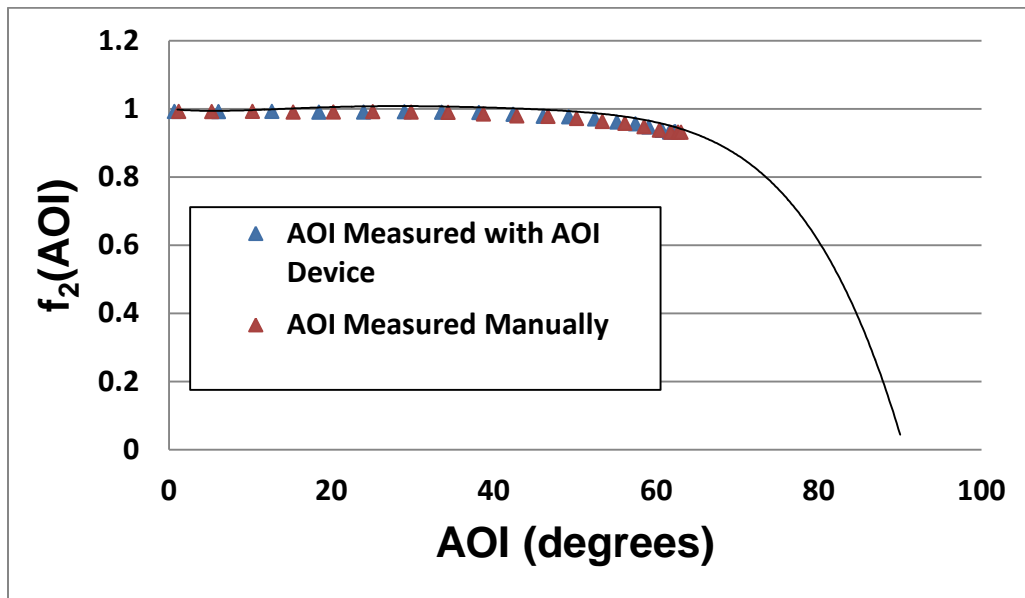


Figure B 1: Comparison of relative optical responses obtained using the AOI hardware and AOI calculation for a CdTe module with glass superstrate for azimuth rotation(direct to global ratio was 0.89)

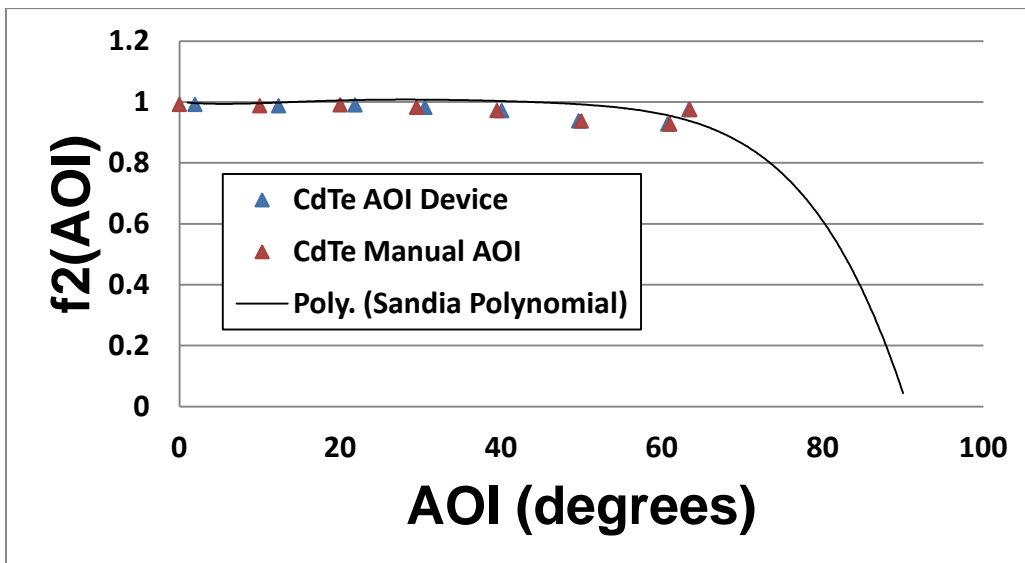


Figure B 2: Comparison of relative optical responses obtained using the AOI hardware and AOI calculation for a CdTe module with glass superstrate for elevation rotation (direct to global ratio was 0.89)

For elevation angle, the two-axis tracker was tilted to the maximum horizontal position of 11° (where 0° is horizontal) and tilted downward to a maximum angle of 74.5°. the f<sub>2</sub>(AOI) data

for elevation angle deviates from the generalized polynomial for higher tilt angles due to the inconsistent reflectance throughout the measurement. When the modules are at  $11^\circ$  tilt (close to horizontal), they 'see' only the sky. As they are tilted downward, the ground reflection could interfere with the data accuracy. This phenomenon does not occur for azimuth angles because the modules are essentially seeing the same ratio of sky and ground (they were at  $30^\circ$  tilt angle for the duration of the azimuth rotation).

The purpose of this experiment was to verify that the manual method and AOI device measurements were consistent. Both methods proved to be accurate. The standard deviation between manually calculated AOI and the AOI device measurement for azimuth angle was  $1.66^\circ$ . The standard deviation between manually calculated AOI and AOI device measurement for elevation tilt was  $1.08^\circ$ .

## **APPENDIX C**

### **ROUND 1: MEASUREMENTS USING A MULTI-CURVE TRACER**



The data presented in the main body (round 3; final round) of the report evolved from previous two rounds of data collections and reductions. Improvements to the experimental setup and data processing were made for each round. For round 1 of data collection, a DayStar (DS3200) multi-curve tracer was used to measure and record  $I_{sc}$ , module temperature, and irradiance sensor readings. The main problems concerning round 1 measurements were:

1. The fastest time the multi-curve tracer could record and store data was one minute intervals. This was due to a software limitation of the multi-curve tracer, not a hardware issue. The multi-curve tracer saves data files onto the hard drive by automatically assigning them a file name based on the time the data was collected. The data file is named only for the hour and minute it is stored (not for the second). The physical capabilities of the tracker allow it to take data for the five modules in ten seconds. However, since the files are automatically assigned a name based on the time they were taken, the minimum time interval the data could be recorded and stored was one minute. For this experiment, the tracker was rotated by  $5^\circ$  AOI every one minute until it reached a maximum of  $77^\circ$  AOI. The experiment was performed in 16 minutes and a total of 16 data points were collected. The 16 data points in 16 minutes is sufficient to comply with the IEC 61853-2 standard which states *for devices with rotational symmetry of the reflectivity with respect to the module normal, do a minimum of 9 different angles to span the angles from 0 to  $80^\circ$  for one direction*. To confidently validate this statement, more data points were needed. Since data should be recorded as quickly as possible to reduce the spectral change during the experiment, round 2 was proposed to be carried out using equipment that could measure and record data in less than one minute intervals.
2. The irradiance sensors used for measuring global irradiance in the plane of array (pyranometers) and direct normal irradiance (pyrheliometer) had not been calibrated, and therefore, the accuracy of the measurements could not be confirmed and the uncertainty could not be calculated.

The relative  $I_{sc}$  obtained versus AOI plot is shown in Figure C1. Using Equation A6 of Sandia, the relative optical response data,  $f_2(AOI)$  data, was plotted (symbol) versus AOI as shown in Figure C2. The plotted data (symbols) was then compared to the “generic” polynomial curve (solid line) empirically derived by Sandia National Laboratories. As can be seen in this figure, there is a significant difference between the  $f_2(AOI)$  data calculated using the experimental data and the generic polynomial curve (between  $60^\circ$  and  $75^\circ$ ). This difference warranted further investigation. A further investigation revealed a human error that was made in constructing the Equation A6 in the Excel spreadsheet. This error was fixed in the final rounds of data processing. Nevertheless, the multi-curve tracer method, as opposed to the transducer/data logger method, was not continued for the second and final rounds of measurements due to the limitation on the number of data points that could be collected during the short duration of tracker rotation.

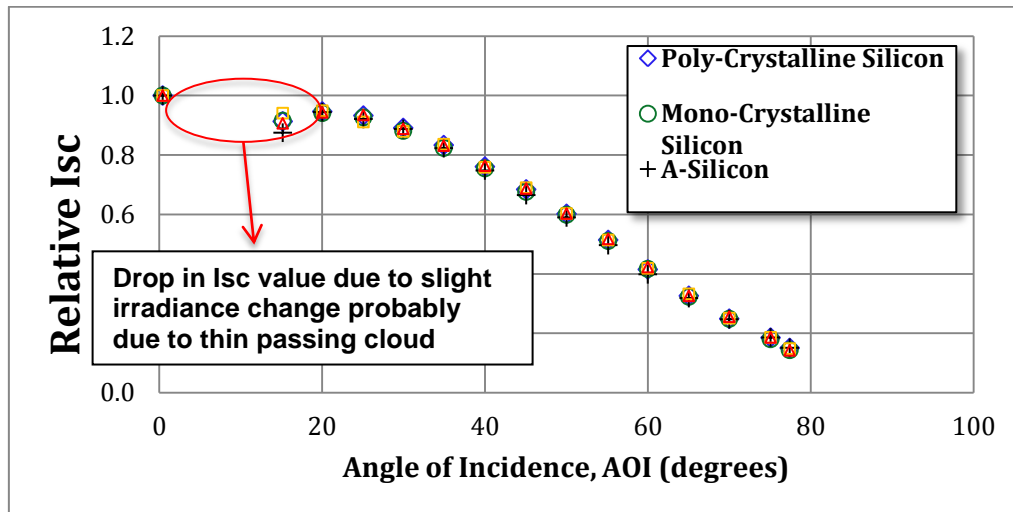


Figure C 1: Round 1 – Relative short circuit current<sup>t</sup> verses AOI for five modules (Multi-curve tracer method)

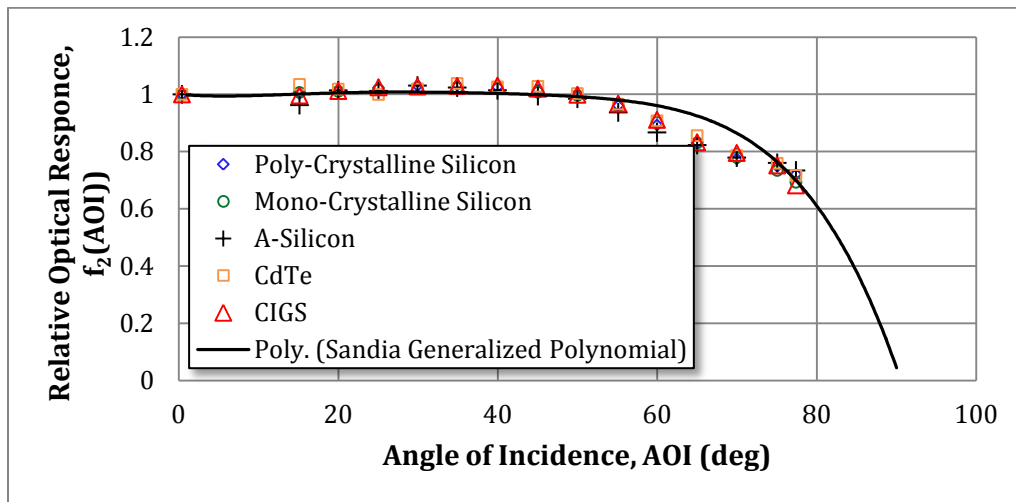


Figure C 2: Round 1 - Data for five modules where  $f_2(AOI)$  was erroneously calculated using Equation A6 (Multi-curve tracer method)

## **APPENDIX D**

### **ROUND 2: MEASUREMENTS USING A TRANSDUCERS AND DATA LOGGER**

The second round of measurement involved the use of CR-magnetic DC transducers and a Campbell scientific CR1000 data logger and multiplexer to measure and collect data for short circuit current, module temperature, and reference cell. Few problems that were detected in the round 1 of measurements were rectified in round 2 and they are as follows:

- 1) Multi-curve tracer was able to collect and store data for every one minute but in round 2, the data logger and multiplexer were able to take and store data for every 30 seconds. In round 2, 16 data points were collected in approximately 9.5 minutes.
- 2) The human error that was present in the MS Excel spreadsheet equation in round 1 was corrected in round 2 and all the plots obtained from round 2 used the correct equation. However, the reference devices were still not calibrated for the experiment, causing a delay in calculating the uncertainty.

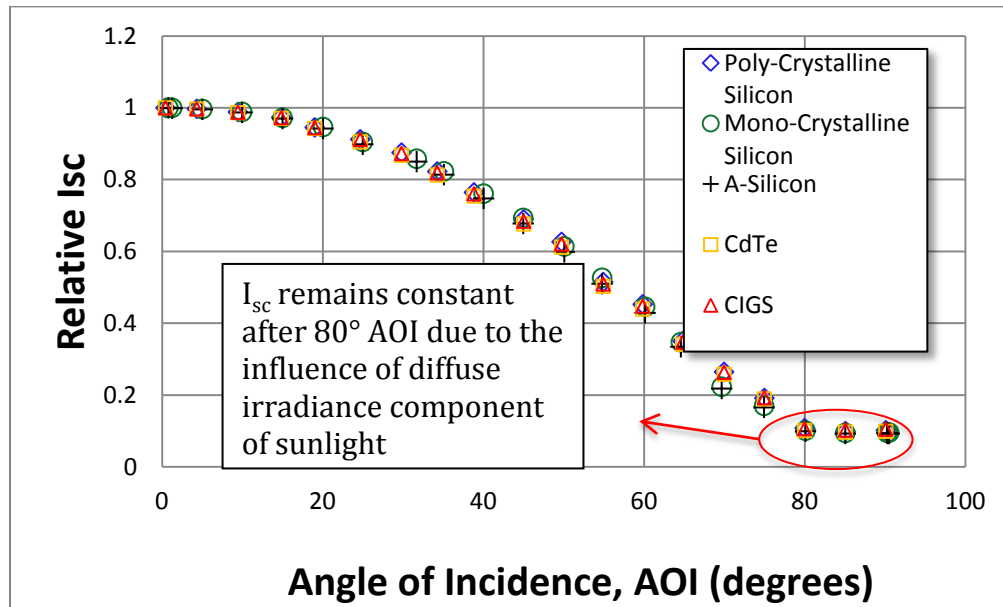


Figure D 1: Round 2 – Relative short circuit current verses AOI for five modules (Data logger method)

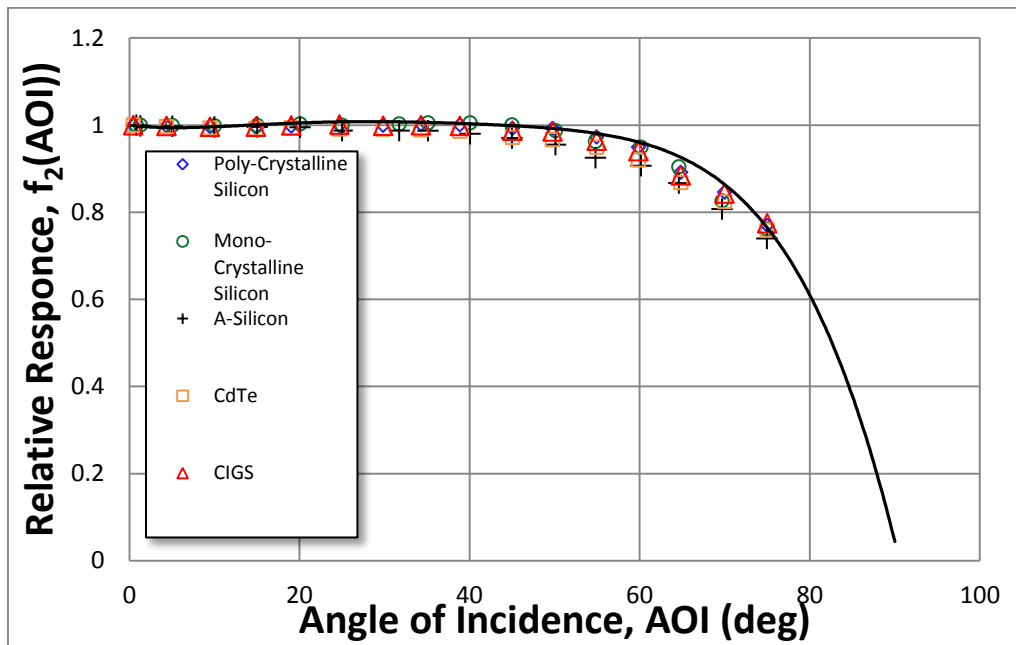


Figure D 2: Round 2 - Data for five modules where  $f_2(\text{AOI})$  was correctly calculated using Equation A6 (Data logger method)

## **APPENDIX E**

### **INTER-COMPARISON AND CROSSCHECKING OF PYRANOMETERS**

For this experiment, a calibrated Eppley PSP pyranometer was cross referenced with a Kipp & Zonen CMP21 pyranometer, to measure global irradiance in the plane of array . The f2 (AOI) calculation proved to be extremely sensitive to the accuracy of the global irradiance measurements. The pyranometers were mounted coplanar to the PV modules and in positions on the tracker so that no shading of the modules or the other reference devices occurred. The E<sub>poa</sub> measurements for both devices were recorded simultaneously by the CR1000 data logger and are shown in Table E1. The AOI experiment was performed on several different days with various ratios of direct normal irradiance to global irradiance (E<sub>dni</sub>/E<sub>poa</sub>). For each case, the standard deviation of the pyranometers' measured global irradiance in the plane of array (E<sub>poa</sub>) increased as AOI increased. Figure E2 gives E<sub>poa</sub> measured for both pyranometers and their standard deviation as measured for an 87% E<sub>dni</sub>/E<sub>poa</sub> ratio.

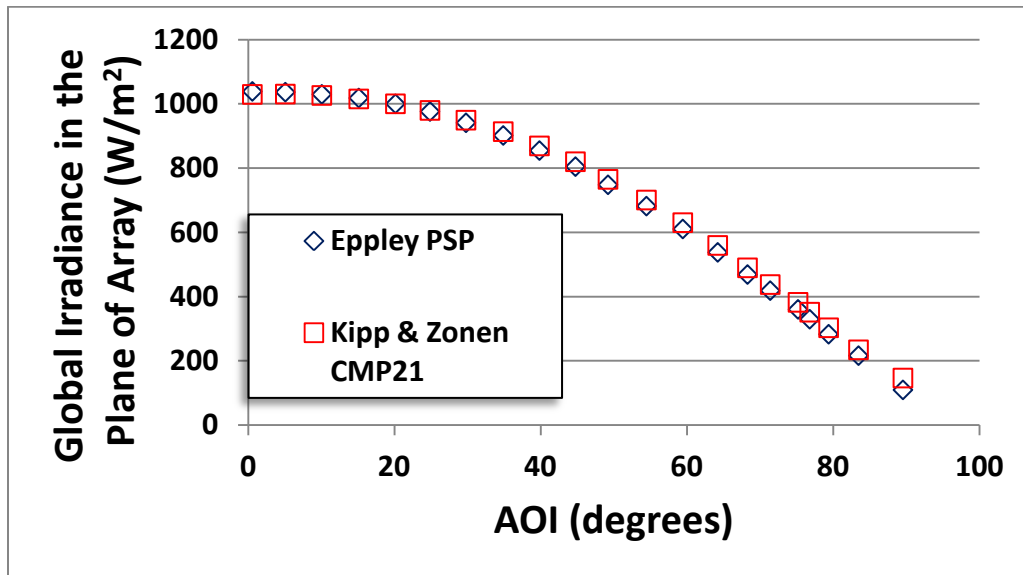


Figure E 1: Global irradiance as measured by the Kipp & Zonen CMP21 and Eppley PSP pyranometer for 87% E<sub>dni</sub>/E<sub>poa</sub>



Table E 1: Comparison of Kipp & Zonen CMP21 versus Eppley PSP measured global irradiance in the plane of array for 87% direct to global irradiance ratio

88% Edni to Epoa Ratio			
AOI (degrees)	Kipp & Zonen Epoa (W/m <sup>2</sup> )	Eppley Epoa (W/m <sup>2</sup> )	Difference (%)
0.6	1029.3	1038.6	0.9%
5.1	1030.3	1036.4	0.6%
10.1	1026.0	1029.5	0.3%
15.1	1015.2	1018.2	0.3%
20.2	1000.0	1000.0	0.0%
24.9	979.4	976.1	0.3%
29.8	949.1	940.9	0.9%
34.9	913.3	901.5	1.3%
39.9	868.9	854.4	1.7%
44.8	819.7	804.4	1.9%
49.2	764.8	747.8	2.3%
54.5	700.4	681.5	2.8%
59.5	629.9	610.2	3.2%
64.2	559.0	537.4	4.0%
68.3	489.3	468.4	4.5%
71.4	437.2	418.3	4.5%
75.2	381.8	359.9	6.1%
76.8	351.1	329.2	6.7%
79.4	302.6	282.5	7.1%
83.5	233.9	215.8	8.4%
89.6	146.0	109.2	33.7%

The data presented above represents the data used in the main body of this report. However, experiments were also performed for other days with various direct to global irradiance ratios. Figure E3 gives a comparison of irradiance data for a direct to global irradiance ratio of 81%. This data also shows a higher standard deviation for higher AOI. For AOI from 0° to 66° the average standard deviation is 4% whereas for AOI from 67° to 90° the average standard deviation is 15%. Figure E5 gives a comparison of irradiance data for an overcast day where the ratio of direct to global irradiance was 2%. For this data, the standard deviation between the two pyranometers remained approximately constant, but higher, for all AOI.

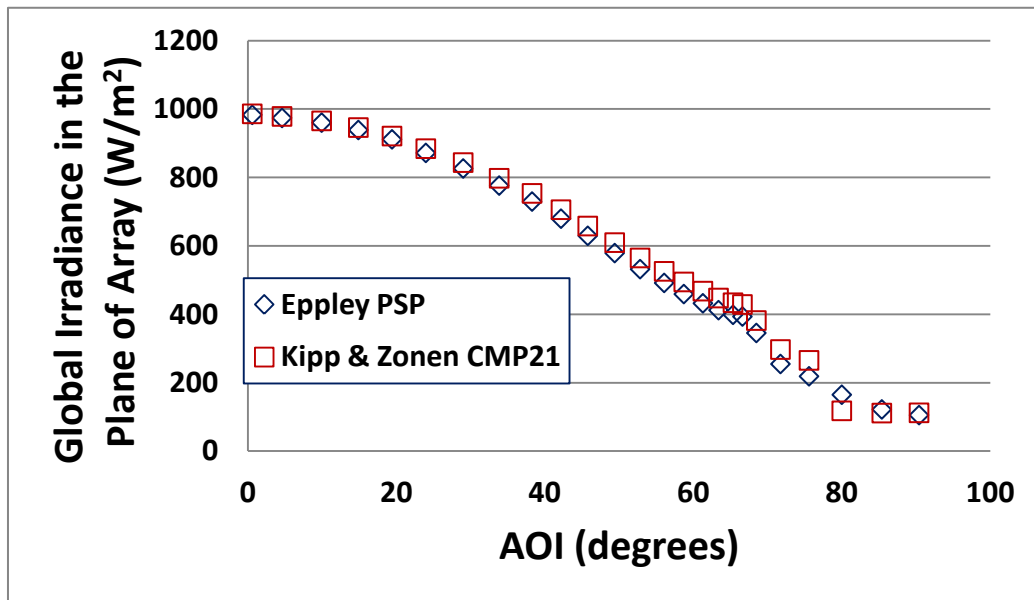


Figure E 2: Comparison of Kipp & Zonen CMP21 verses Eppley PSP measured global irradiance in the plane of array for 81% direct to global irradiance ratio

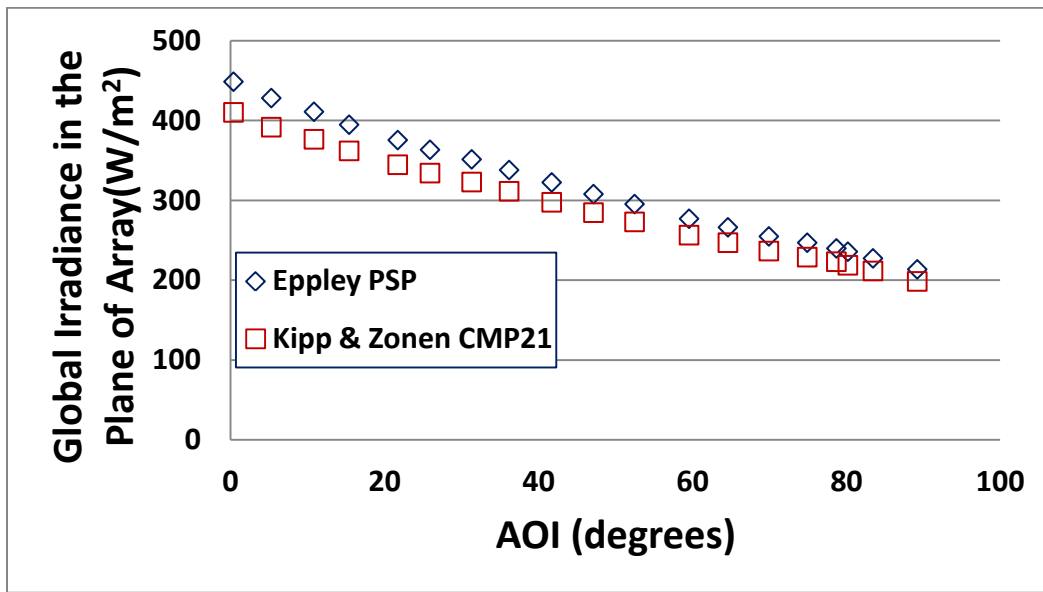


Figure E 3: Comparison of Kipp & Zonen CMP21 versus Eppley PSP measured global irradiance in the plane of array for 2% direct to global irradiance ratio.

## **APPENDIX F**

MEASUREMENT OF  $f_2(\text{AOI})$  VERSES AOI IN THE OPPOSITE DIRECTION

Standard IEC 61853-2 (draft) called for the verification of rotational symmetry of the reflectivity with respect to the module normal. First, the data was collected by rotating the tracker from west (starting at  $0.59^\circ$  AOI) to the east (ending at  $83.50^\circ$ ) within ten minutes. Then the tracker was set to automatic mode and was tracking from east to west. By using the Sandia equation A6 a graph was plotted as shown in Figure F1.

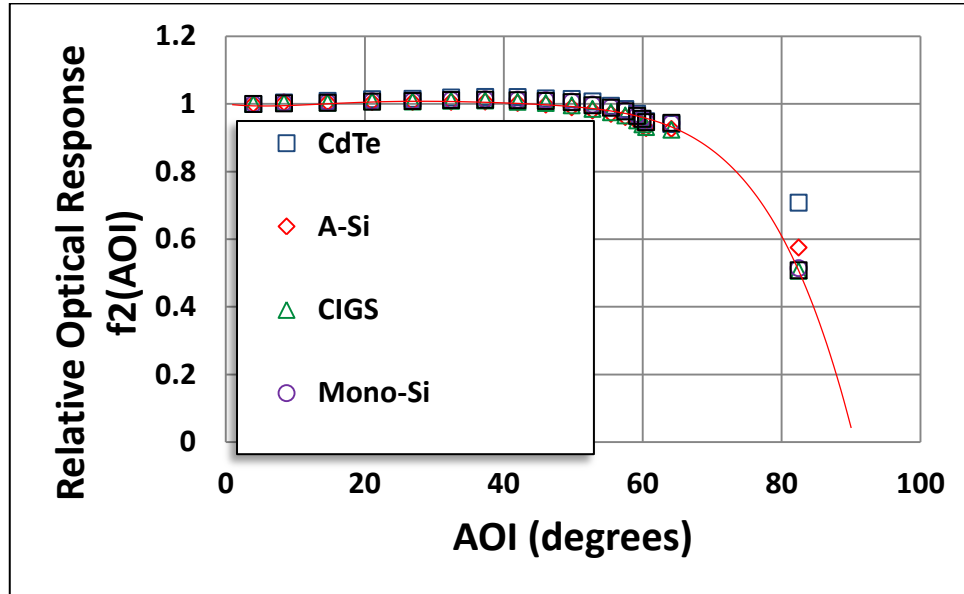


Figure F 1: Round 3 - Data for five modules where  $f_2(AOI)$  was calculated when the tracker was rotated in the opposite direction (East to West)

There were a few disadvantages noted while allowing the tracker to track in the automatic mode. While doing the test in the manual mode, the tracker was rotated both in azimuth and elevation proportionally. When the tracker is allowed to track back, the elevation angle is adjusted first and then rotates in the azimuth. However, the relative optical response of the module is not affected. The AOI changes faster when the tracker is tilted in the elevation than rotating the tracker azimuthally. Since the tracker was rotated in the elevation for the first 30 seconds, the AOI of  $83^\circ$  at 14:37:30 and  $63^\circ$  at 14:38:00 were able to be recorded. After adjusting for the elevation, the tracker was able to rotate azimuthally and hence more data points were able to be collected.

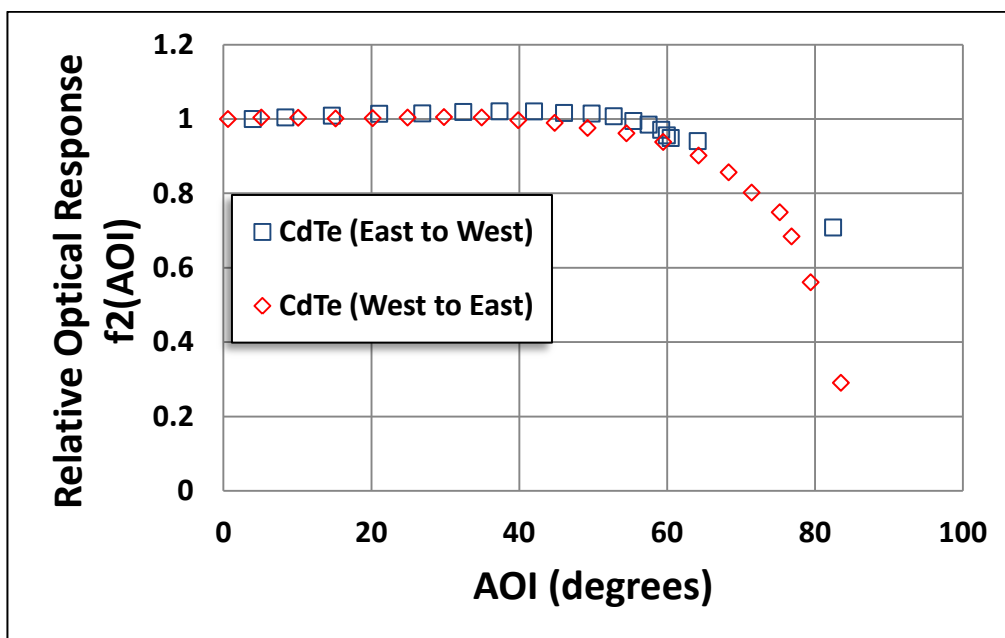


Figure F 2: Round 3 - Data for  $f_2(AOI)$  calculated for CdTe from West to East compared to data when the tracker was rotated in the opposite direction (East to West)

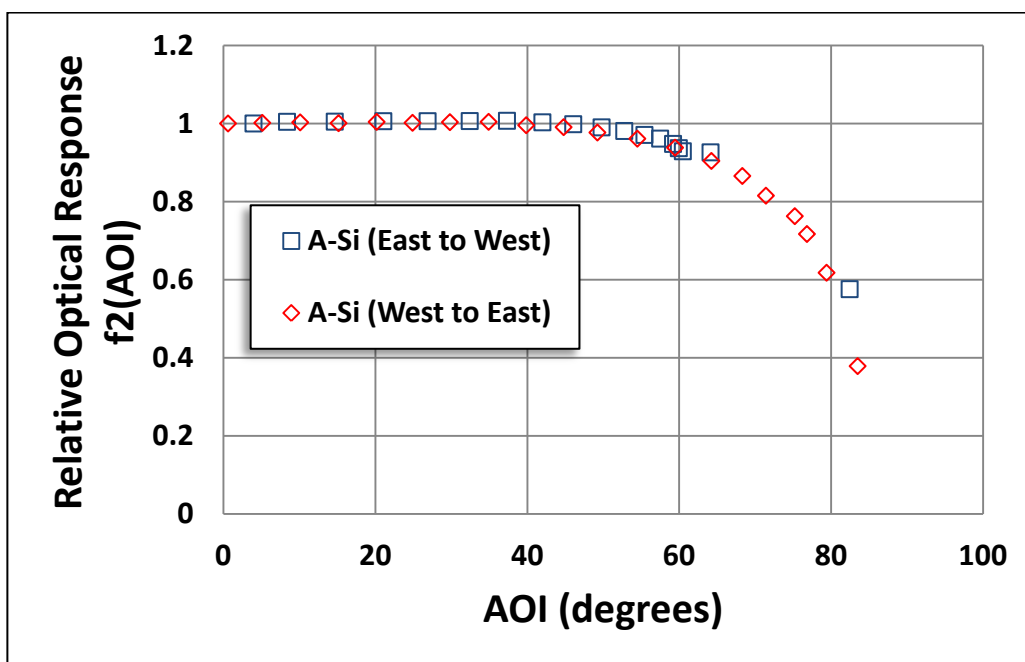


Figure F 3: Round 3 - Data for  $f_2(AOI)$  calculated for a-Si from West to East compared to data when the tracker was rotated in the opposite direction (East to West)

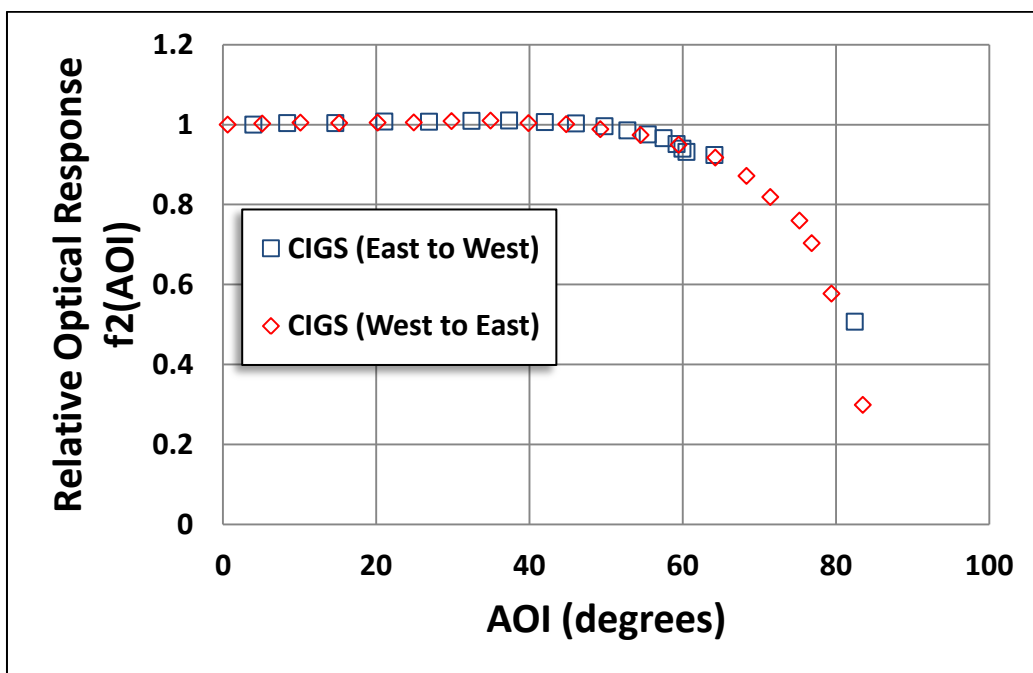


Figure F 4: Round 3 - Data for  $f_2(AOI)$  calculated for CIGS from West to East compared to data when the tracker was rotated in the opposite direction (East to West)

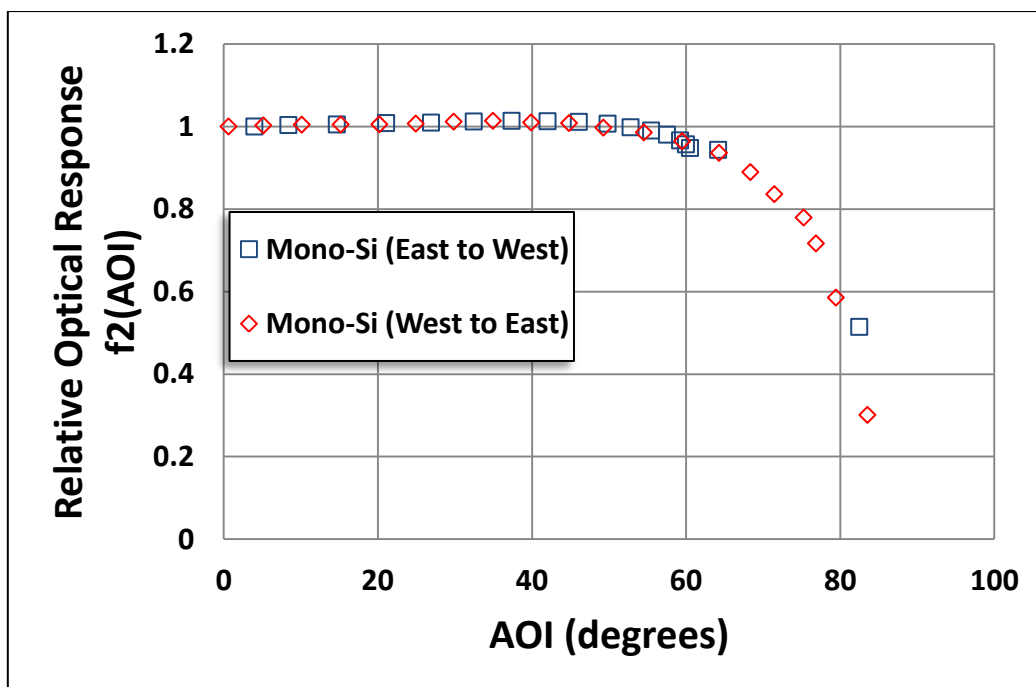


Figure F 5: Round 3 - Data for  $f_2(AOI)$  calculated for Mono-Si from West to East compared to data when the tracker was rotated in the opposite direction (East to West)

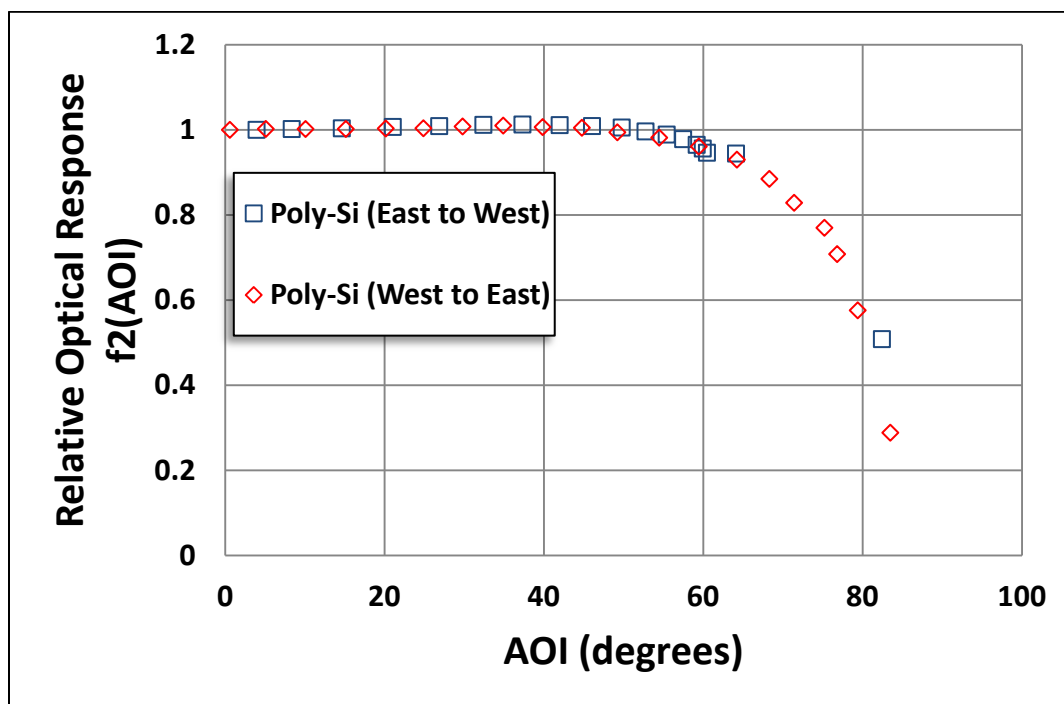


Figure F 6: Round 3 - Data for  $f_2(\text{AOI})$  calculated for Poly-Si from West to East compared to data when the tracker was rotated in the opposite direction (East to West)



## **APPENDIX G**

### **GRAPHICAL METHOD FOR FINDING THE PARAMETER CAUSING DROP IN POWER**

The plots shown below clearly give an idea for determining the parameter causing power degradation, however, the statistical approach for analysis is recommended. The parameter that increases linearly with the drop in power is the factor affecting power degradation.

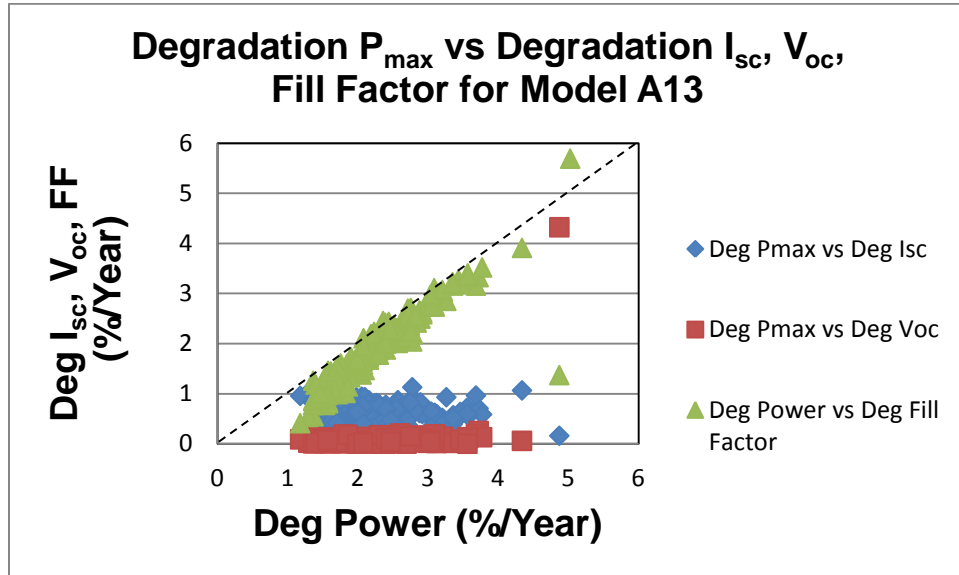


Figure G 1: Degradation power versus degradation of I-V parameters for model A13

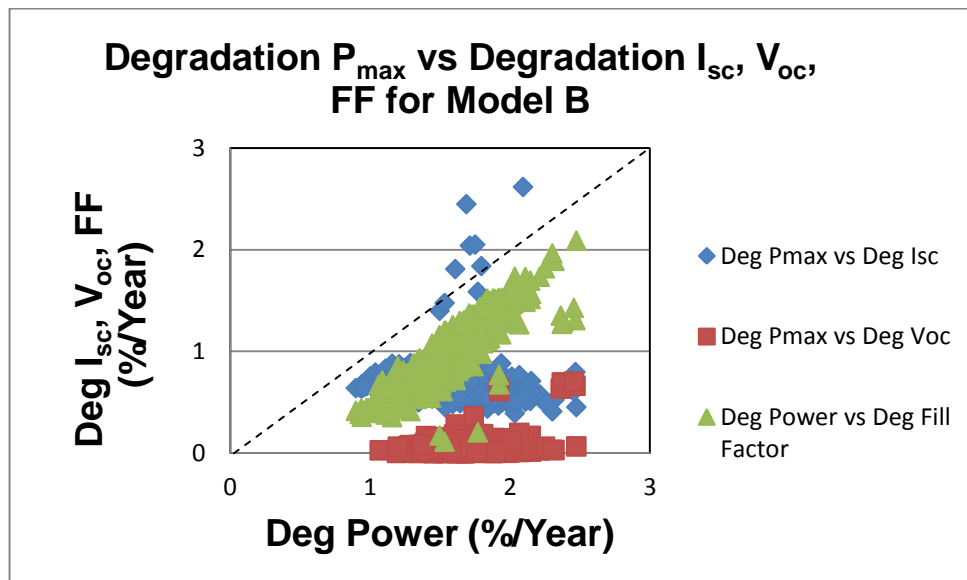


Figure G 2: Degradation power versus degradation of I-V parameters for Model B

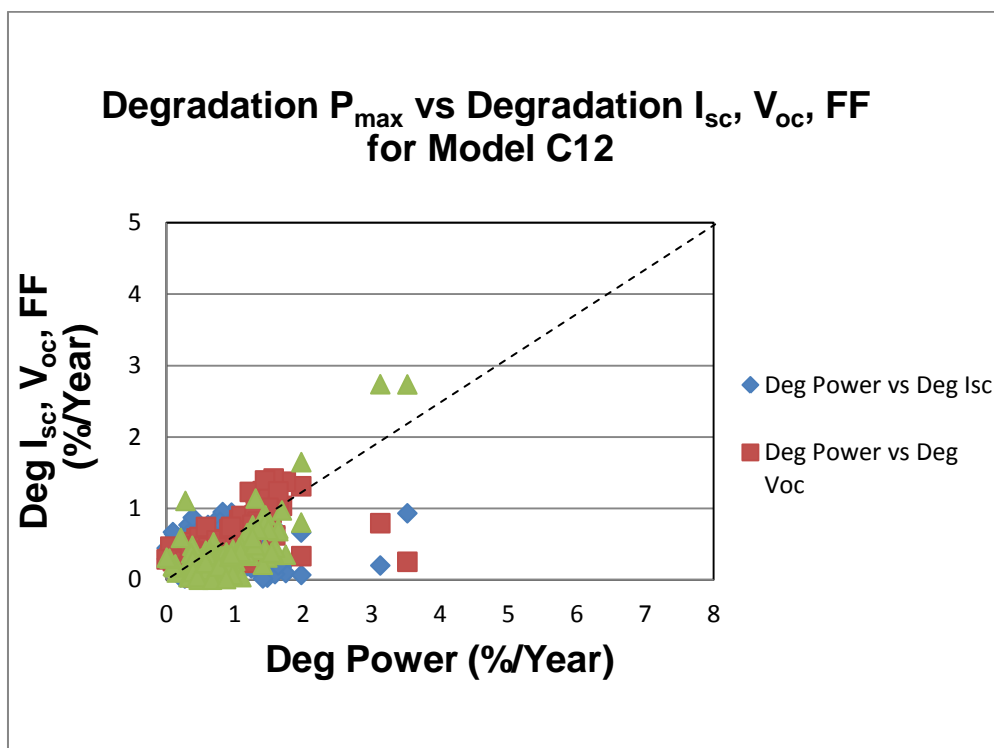


Figure G 3: Degradation power versus degradation of I-V parameters for model C12

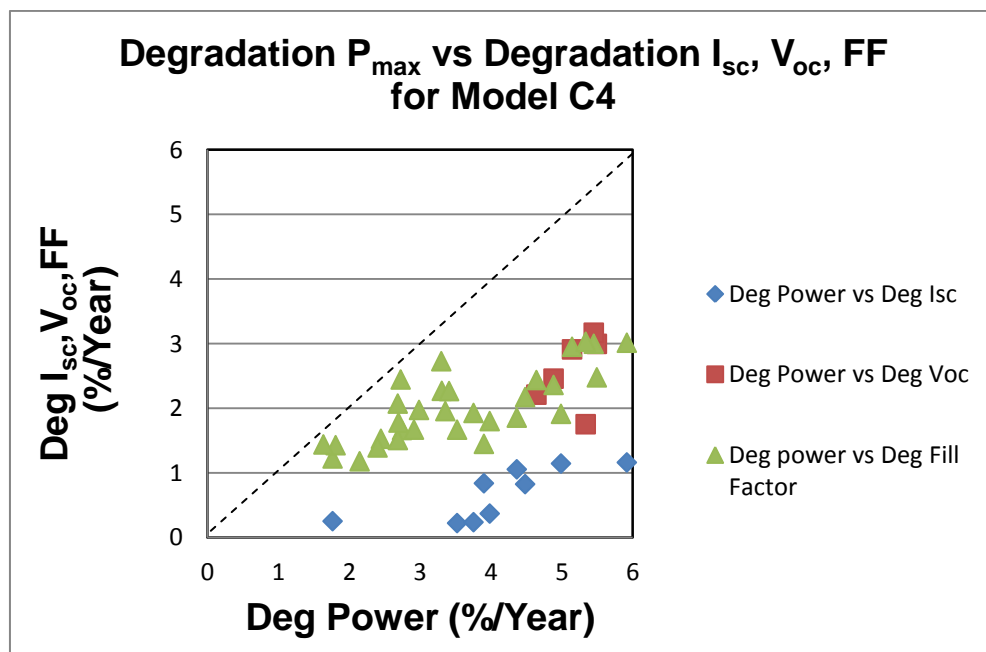


Figure G 4: Degradation power versus degradation of I-V parameters for Model C4

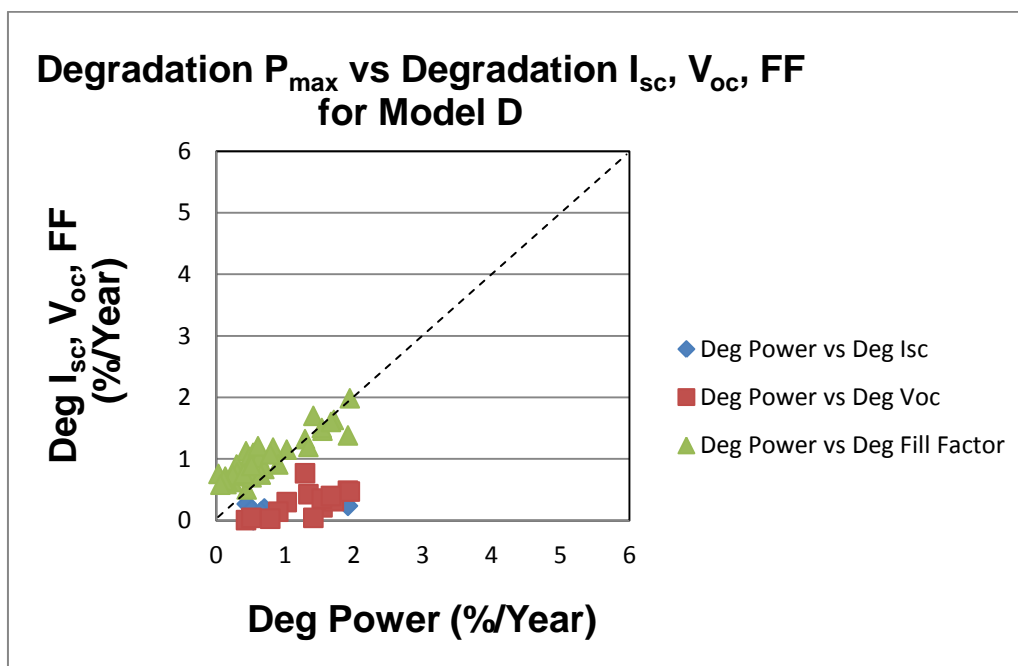


Figure G 5: Degradation power versus degradation of I-V parameters for Model D

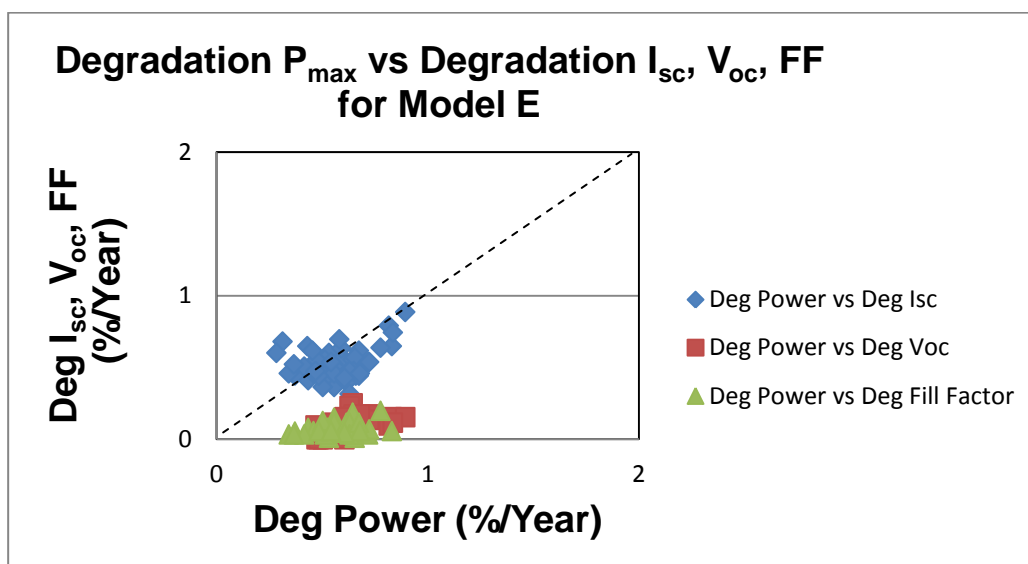


Figure G 6: Degradation power versus degradation of I-V parameters for Model E

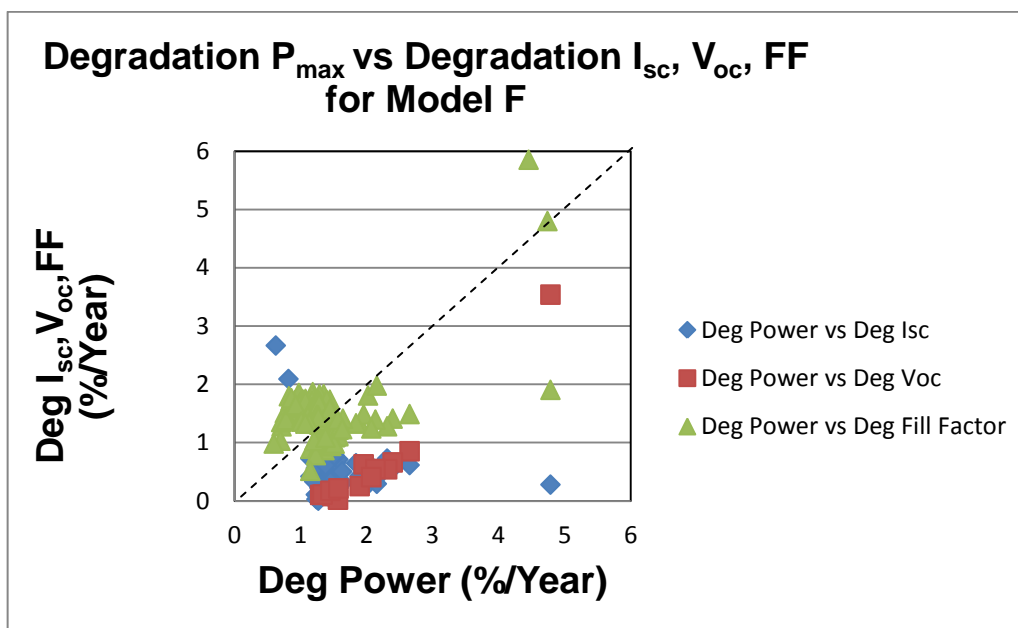


Figure G 7: Degradation power versus degradation of I-V parameters for Model F

## **APPENDIX H**

PARETO CHART OF DEFECTS IN MODULES FOR EACH TYPE OF MODEL

In order to find the primary visual defect that accounts for the drop in power, visual inspection data for each model was obtained from previous researcher's database and was constructed as a Pareto chart in Minitab software. The Pareto chart is a pictorial representation giving the frequency and percentage of occurrence of an observation. The Pareto chart of defects for each type of model is given below.

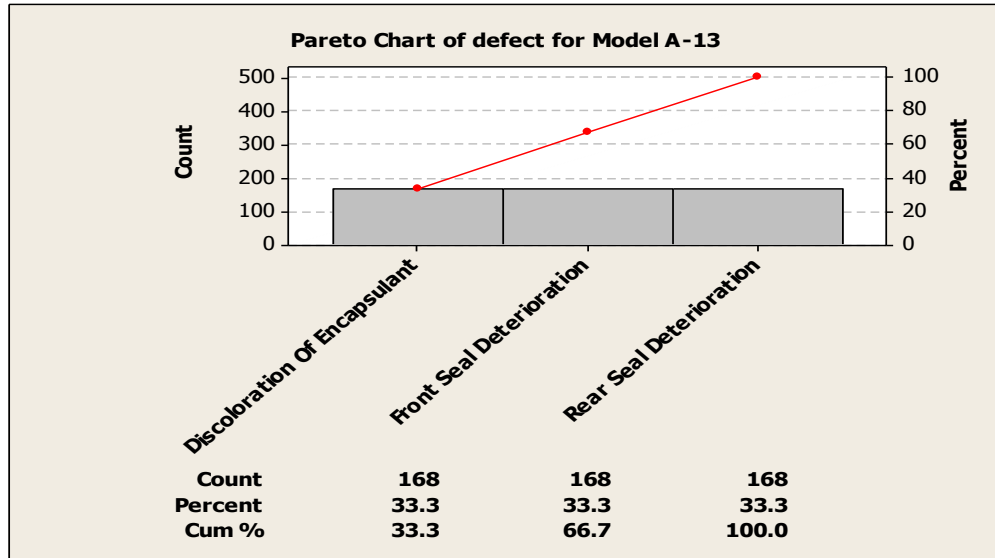


Figure H 1: Pareto chart of defects for Model A13

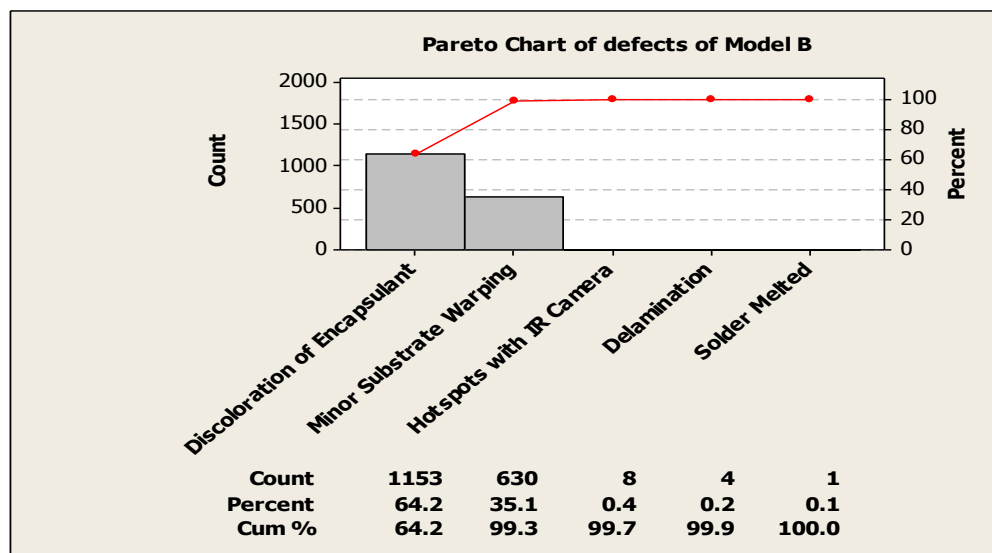


Figure H 2: Pareto chart of defects for Model B

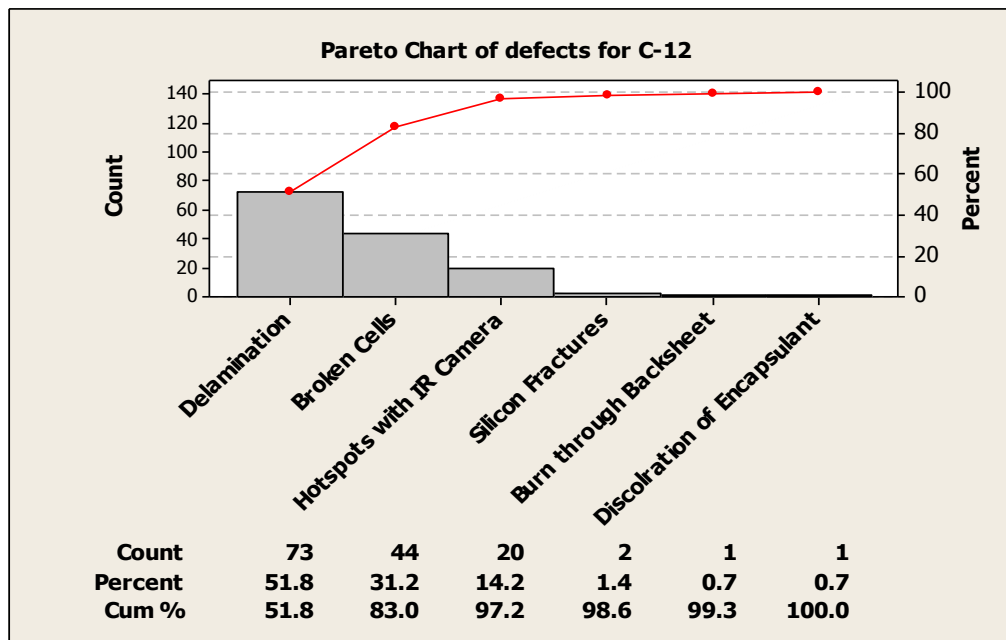


Figure H 3: Pareto chart of defects for Model C12

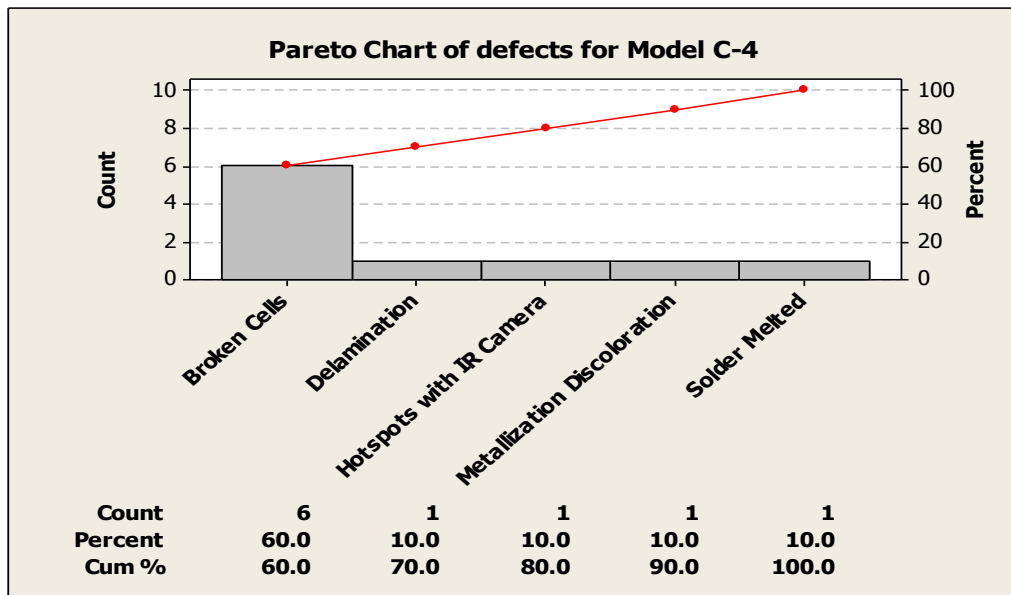


Figure H 4: Pareto chart of defects for Model C4



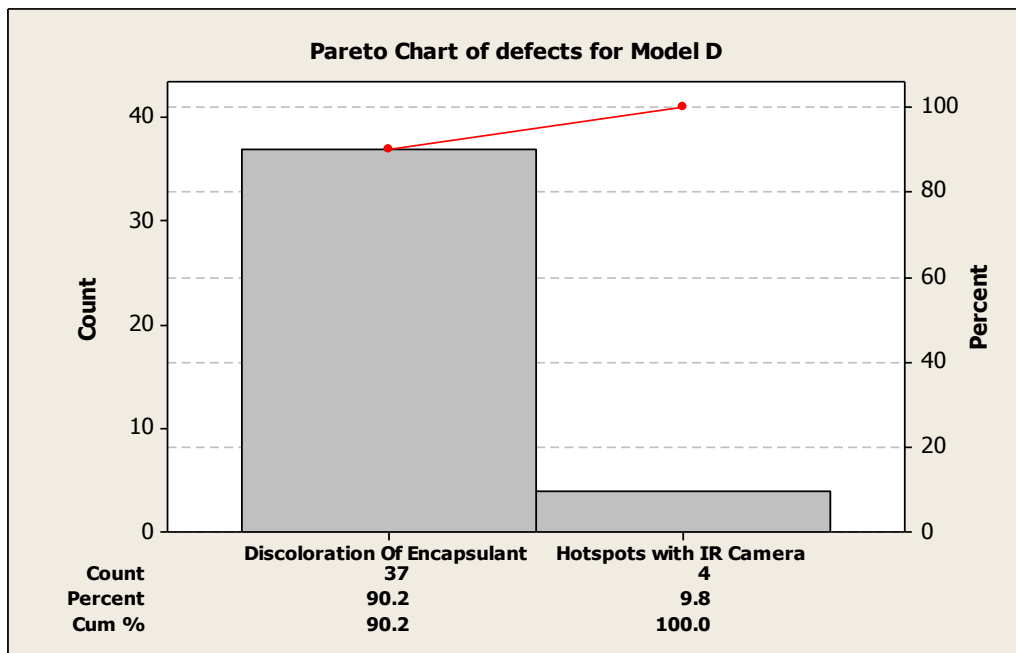


Figure H 5: Pareto chart of defects for Model D

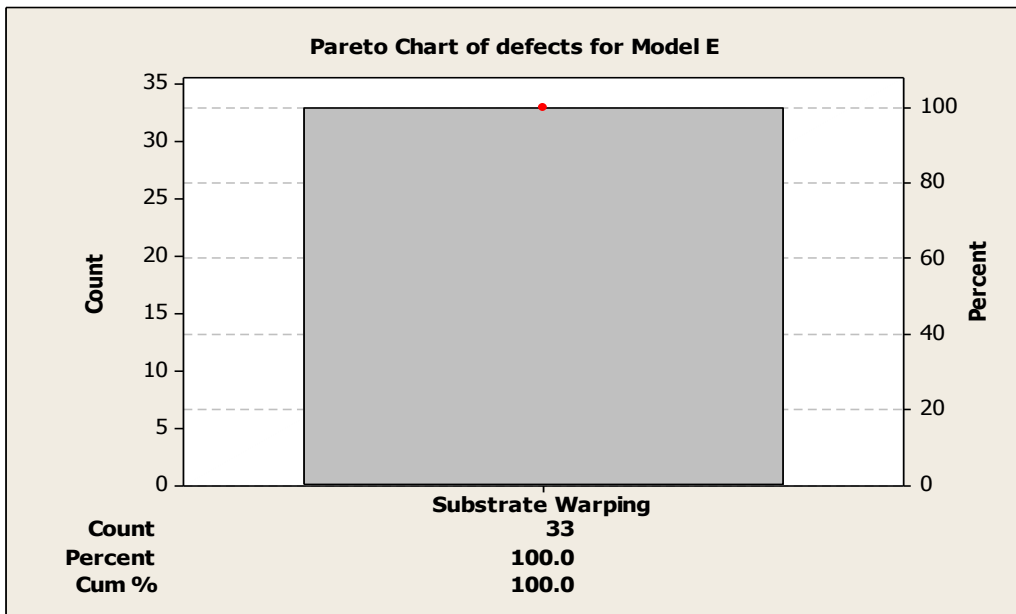


Figure H 6: Pareto chart of defects for Model E

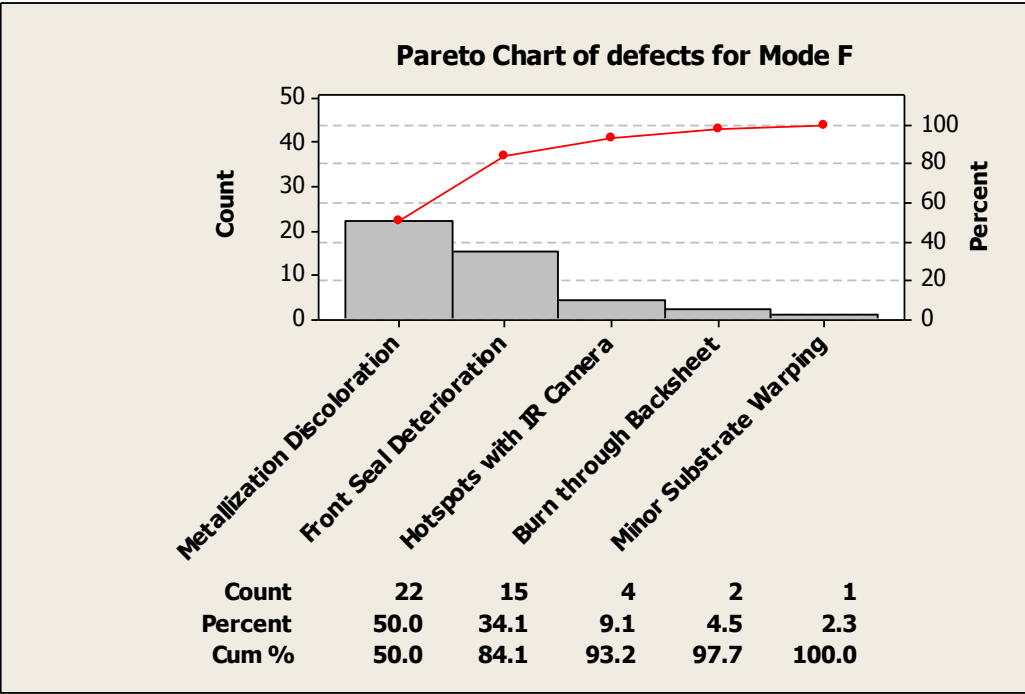


Figure H 7: Pareto chart of defects for Model F

## **APPENDIX I**

### **ANNUAL AVERAGE DEGRADATION RATE FOR I-V PARAMETERS FOR ALL MODELS**

The plots for annual average degradation of I-V parameters for each model are shown as below.

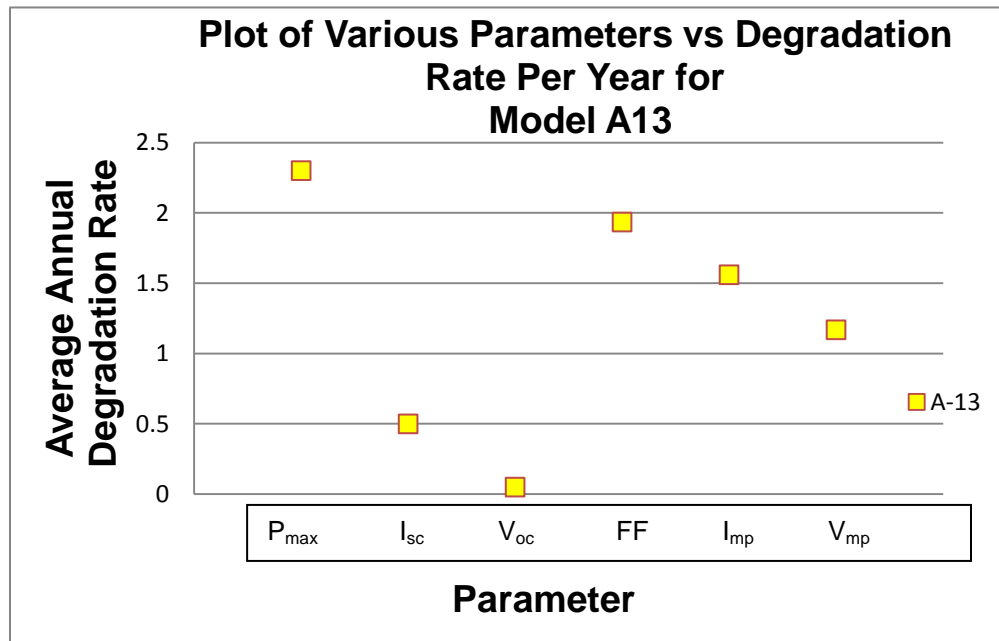


Figure I 1: Plot for average annual degradation of I-V parameters for Model A13

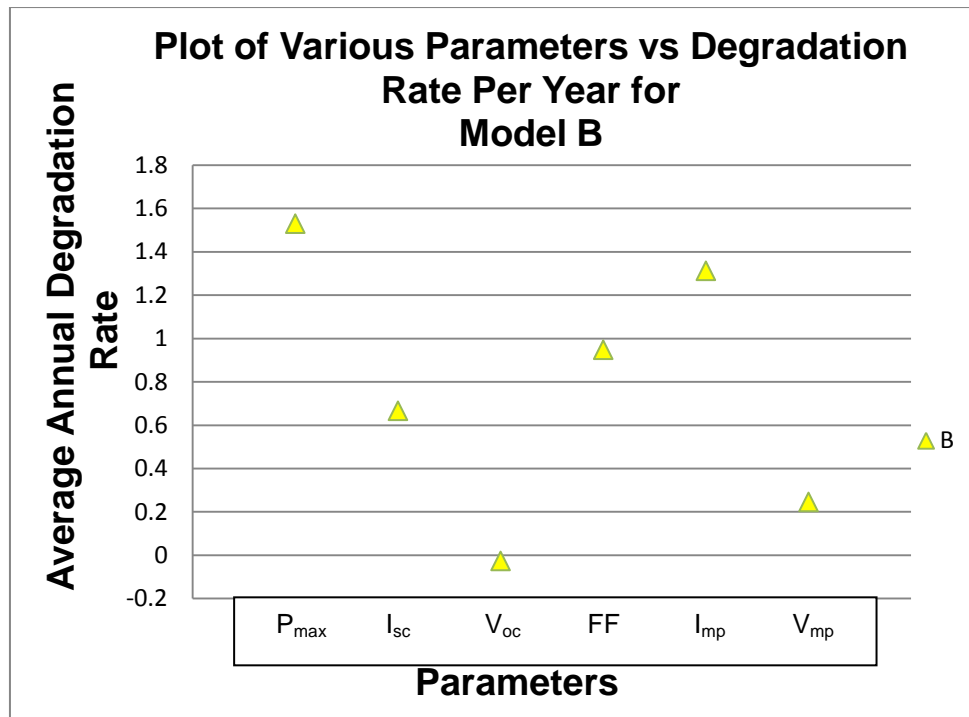


Figure I 2: Plot for average annual degradation of I-V parameters for Model B

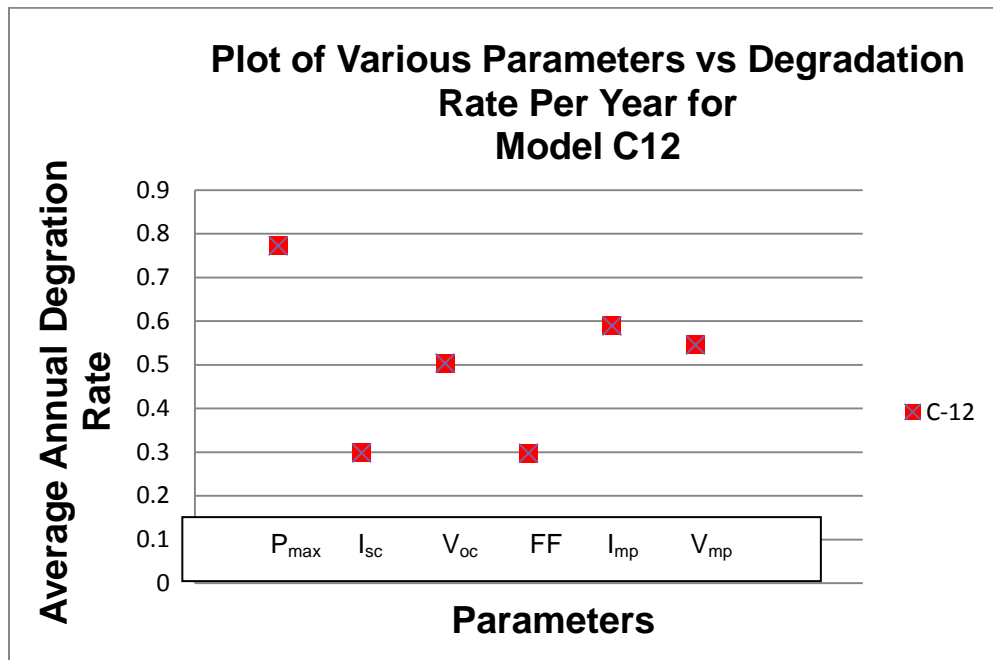


Figure I 3: Plot for average annual degradation of I-V parameters for Model C12

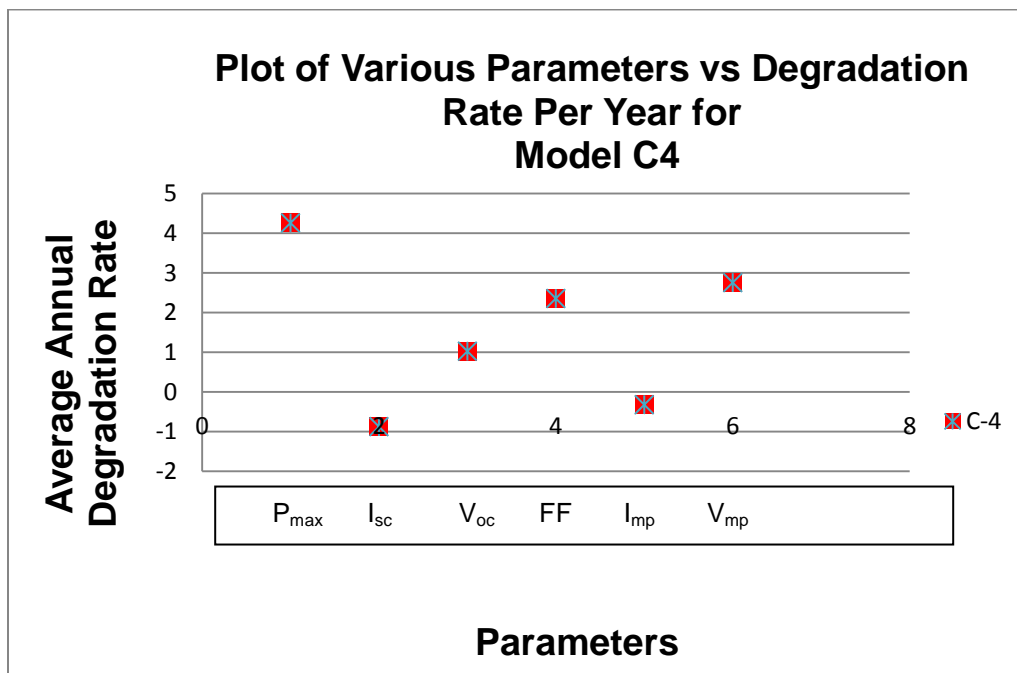


Figure I 4: Plot for average annual degradation of I-V parameters for Model C4

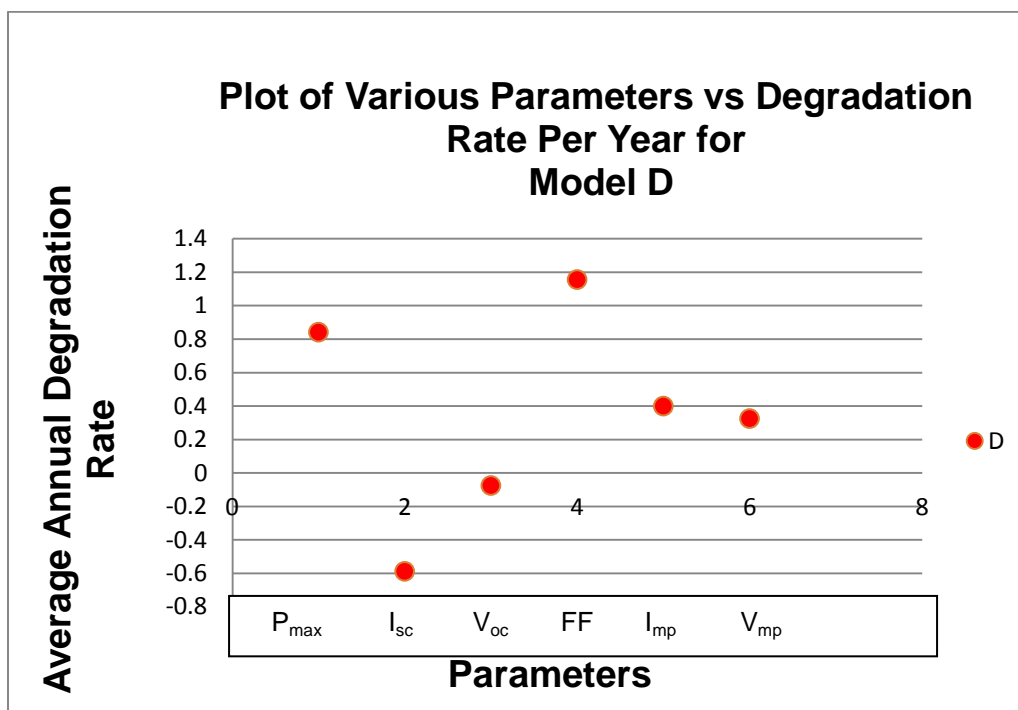


Figure I 5: Plot for average annual degradation of I-V parameters for Model D

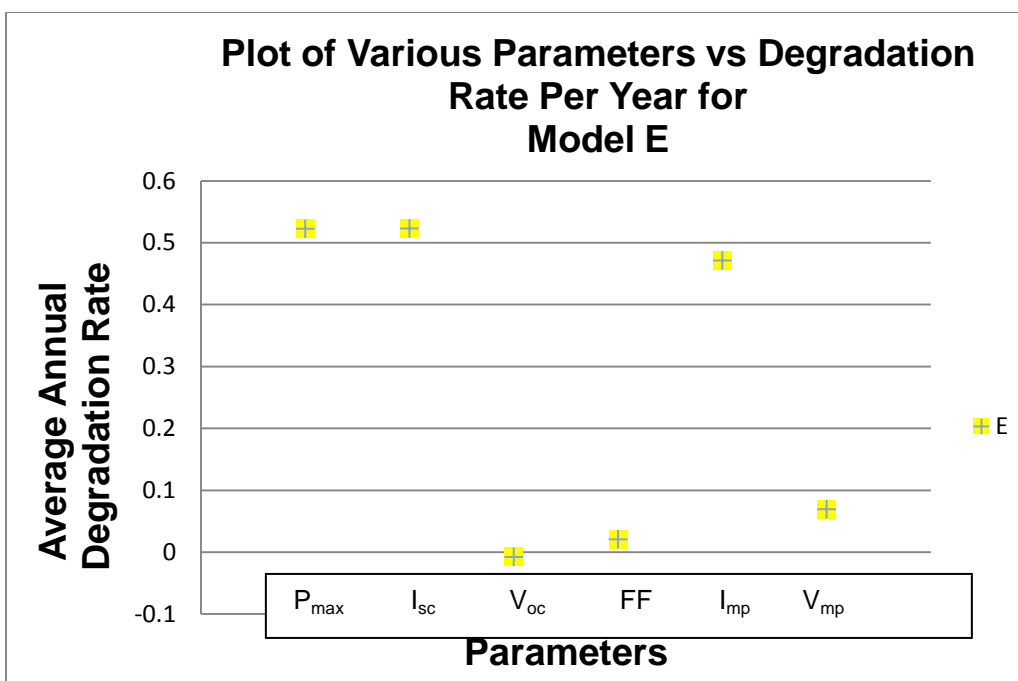


Figure I 6: Plot for average annual degradation of I-V parameters for Model E

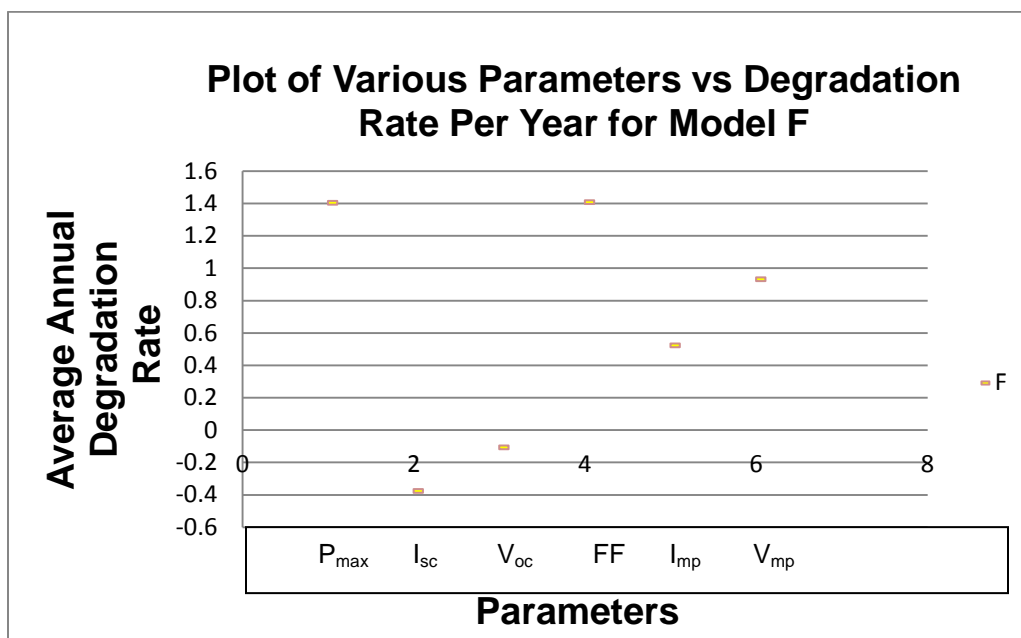


Figure I 7: Plot for average annual degradation of I-V parameters for Model F

## **APPENDIX J**

### **HISTOGRAMS OF POWER DEGRADATION FOR VARIOUS MODELS**



The histograms of power degradation for the models in the power plant are as follows:

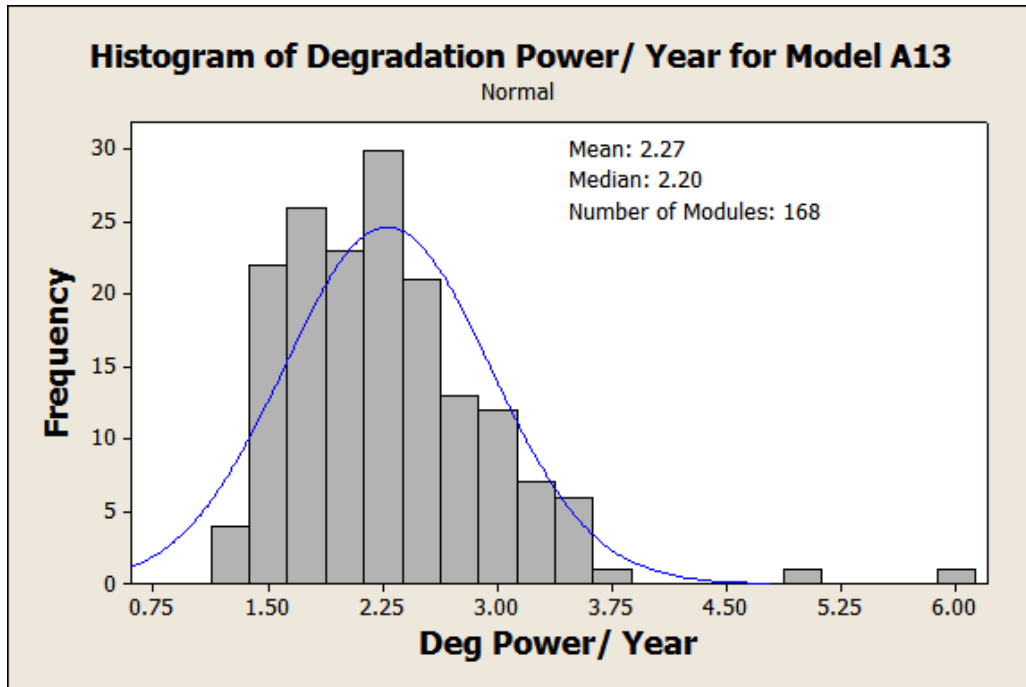


Figure J 1: Histogram of Power Degradation (%/Year) for Model A13

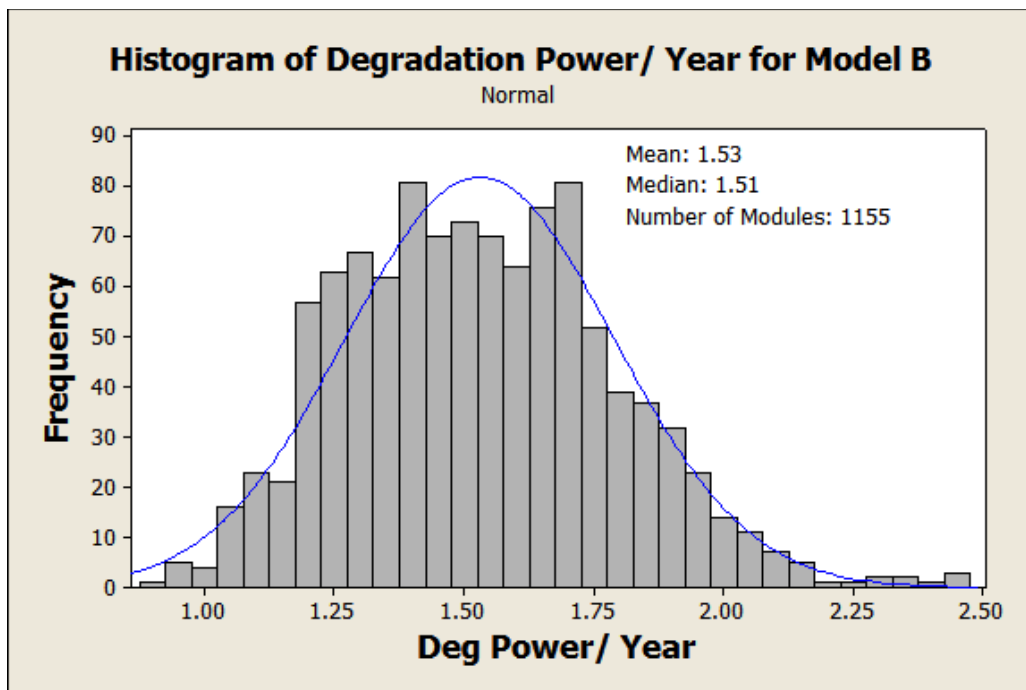


Figure J 2: Histogram of Power Degradation (%/Year) for Model B

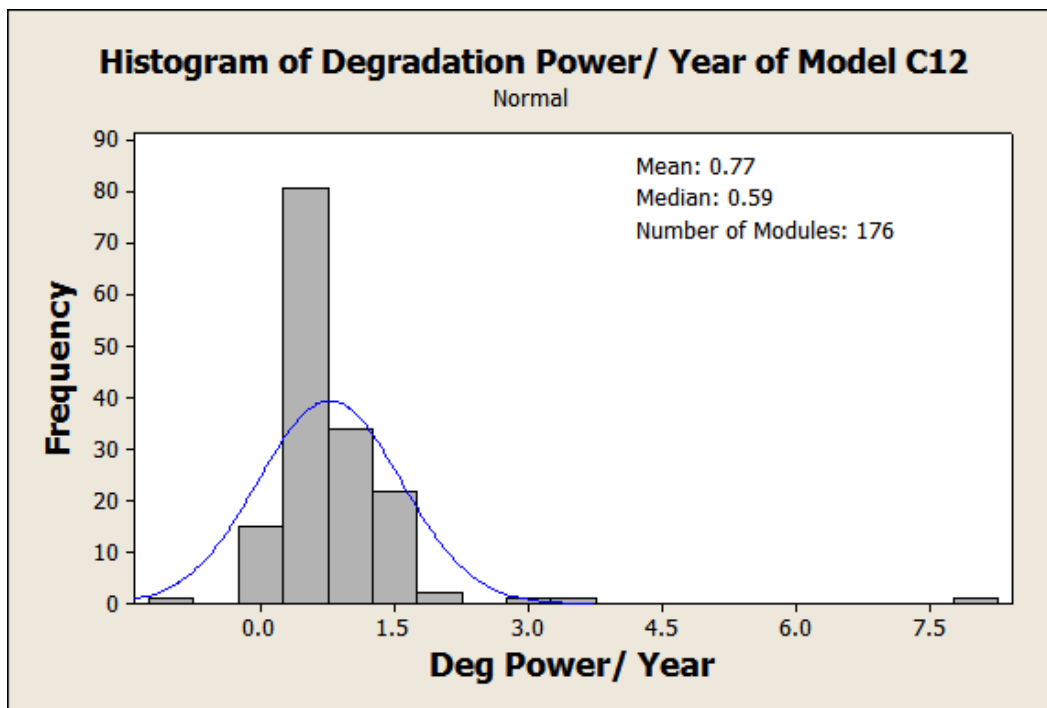


Figure J 3: Histogram of Power Degradation (%/Year) for Model C12

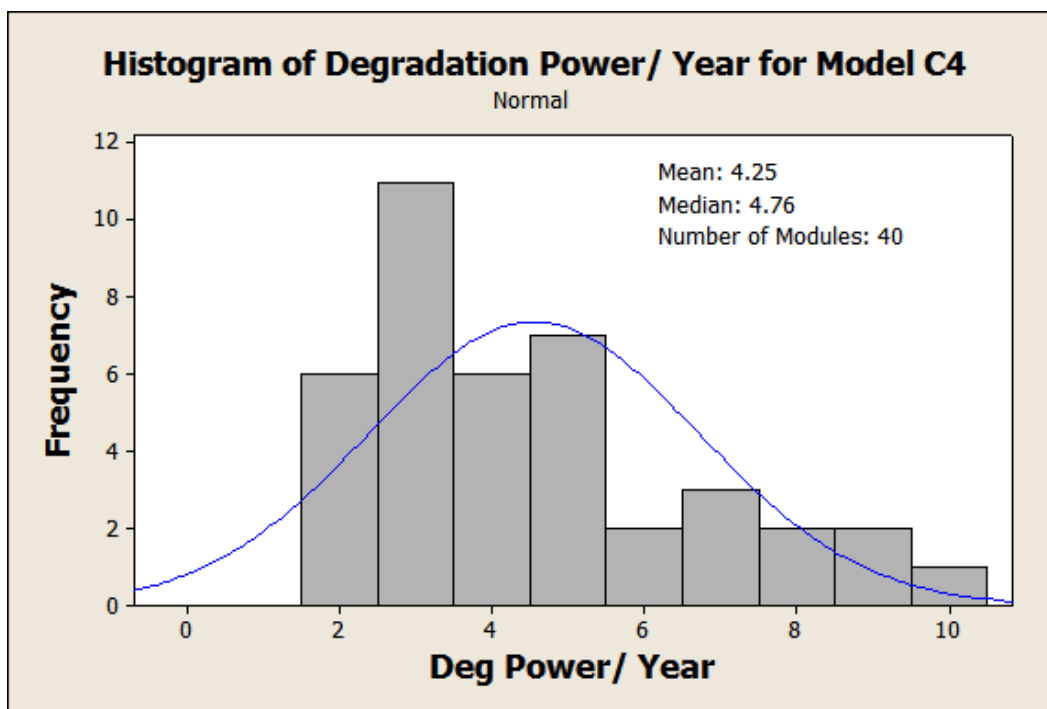


Figure J 4: Histogram of Power Degradation (%/Year) for Model C4

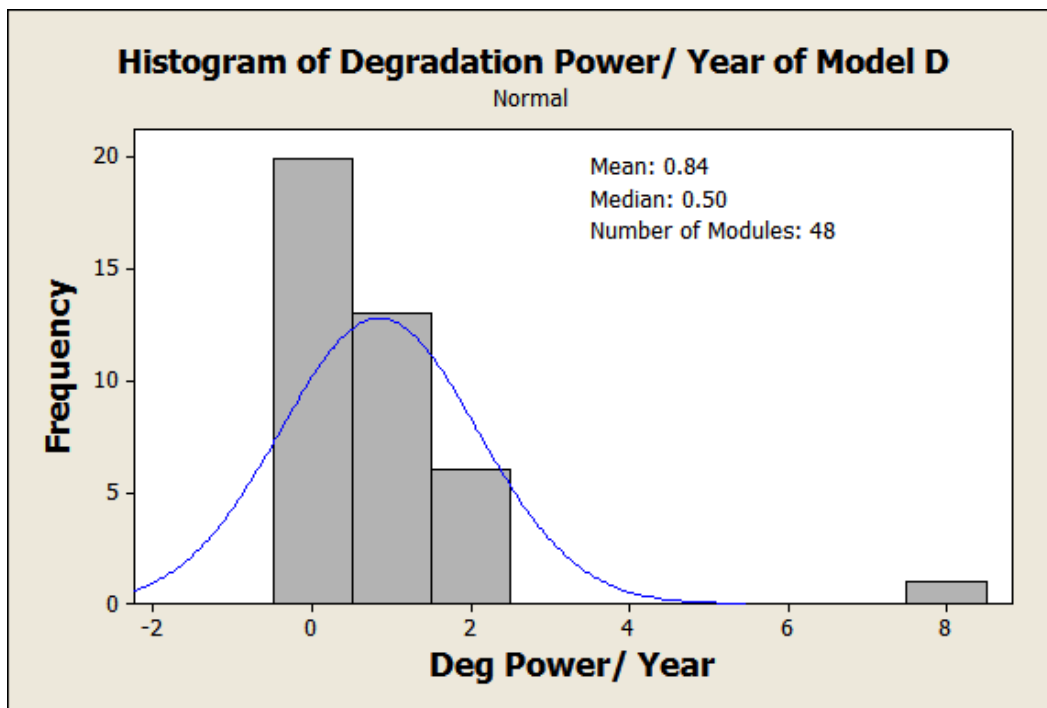


Figure J 5: Histogram of Power Degradation (%/Year) for Model D

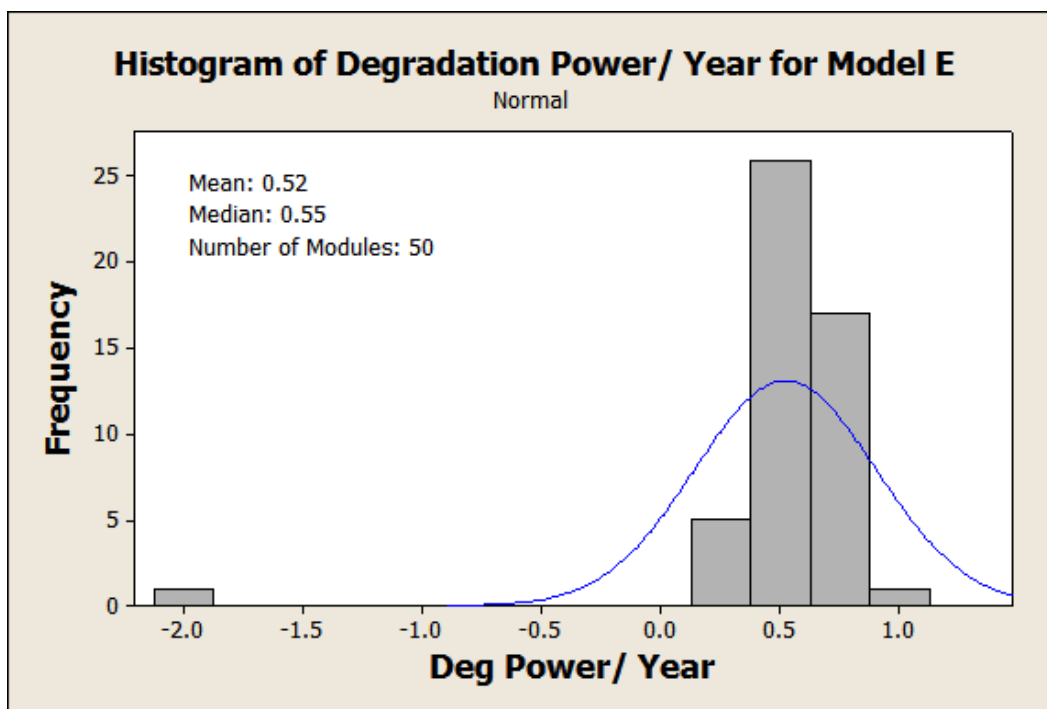


Figure J 6: Histogram of Power Degradation (%/Year) for Model E

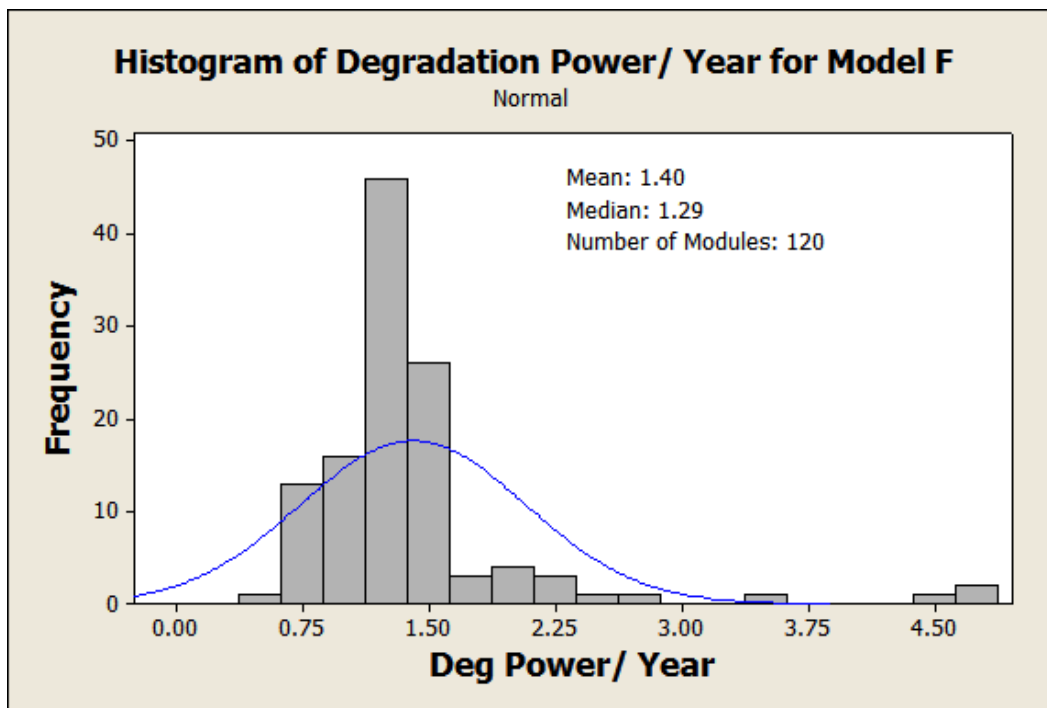


Figure J 7: Histogram of Power Degradation (%/Year) for Model F

## **APPENDIX K**

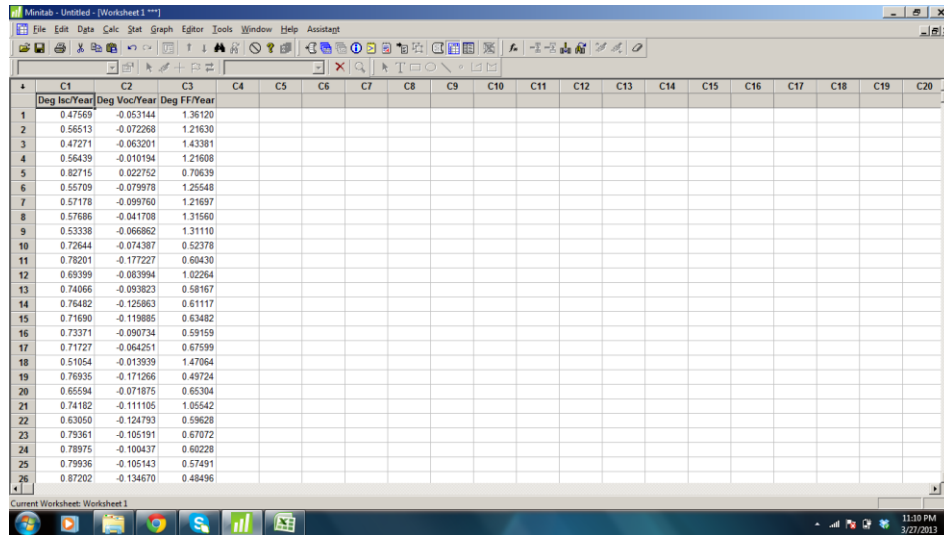
### **SAMPLE HYPOTHESIS TESTING USING MINITAB SOFTWARE**

**STEP 1:** The null and alternative hypotheses are defined.

Null hypothesis: Degradation  $I_{sc}/\text{Year}$ = Degradation FF/year

Alternative hypothesis: Degradation  $I_{sc}/\text{Year}$ = Degradation  $V_{oc}/\text{Year}$

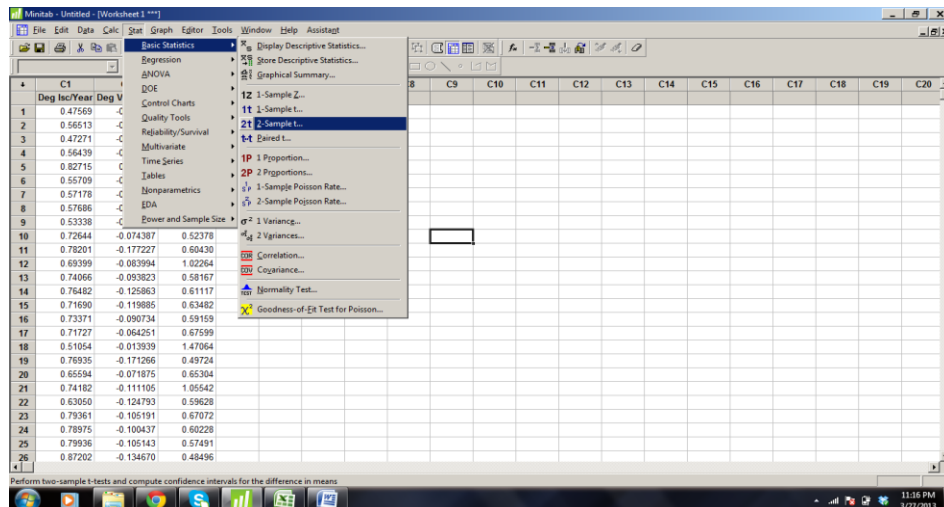
The degradation values of  $I_{sc}$ ,  $V_{oc}$  and Fill Factor per year are collected for Model B



	C1	C2	C3	C4	C5	C6	C7	C8	C9	C10	C11	C12	C13	C14	C15	C16	C17	C18	C19	C20
	Deg Inc/Year	Deg Voc/Year	Deg FF/Year																	
1	0.47569	-0.053144	1.36120																	
2	0.56513	-0.072268	1.21630																	
3	0.47271	-0.063201	1.43381																	
4	0.56439	-0.010194	1.21608																	
5	0.82715	0.022752	0.70639																	
6	0.55709	-0.079978	1.25548																	
7	0.57178	-0.099760	1.21697																	
8	0.57686	-0.041708	1.31560																	
9	0.53338	-0.066862	1.31110																	
10	0.72644	-0.074387	0.52378																	
11	0.78201	-0.177227	0.60430																	
12	0.69399	-0.083994	1.02264																	
13	0.74066	-0.093823	0.58167																	
14	0.76482	-0.125863	0.61117																	
15	0.71690	-0.119885	0.63482																	
16	0.73371	-0.090734	0.59159																	
17	0.71727	-0.064251	0.67599																	
18	0.51054	-0.012939	1.47064																	
19	0.76935	-0.171266	0.49724																	
20	0.65594	-0.071875	0.65304																	
21	0.74182	-0.111105	1.05542																	
22	0.63050	-0.124793	0.59628																	
23	0.79361	-0.105191	0.67072																	
24	0.78975	-0.100437	0.60228																	
25	0.79936	-0.105143	0.57491																	
26	0.87202	-0.134670	0.48496																	

Figure K 1: Degradation values of  $I_{sc}$ ,  $V_{oc}$  and Fill Factor per year pasted on Minitab Software Worksheet

**STEP2:**



	C1	C2	C3	C4	C5	C6	C7	C8	C9	C10	C11	C12	C13	C14	C15	C16	C17	C18	C19	C20
	Deg Inc/Year	Deg Voc/Year	Deg FF/Year																	
1	0.47569	-0.053144	1.36120																	
2	0.56513	-0.072268	1.21630																	
3	0.47271	-0.063201	1.43381																	
4	0.56439	-0.010194	1.21608																	
5	0.82715	0.022752	0.70639																	
6	0.55709	-0.079978	1.25548																	
7	0.57178	-0.099760	1.21697																	
8	0.57686	-0.041708	1.31560																	
9	0.53338	-0.066862	1.31110																	
10	0.72644	-0.074387	0.52378																	
11	0.78201	-0.177227	0.60430																	
12	0.69399	-0.083994	1.02264																	
13	0.74066	-0.093823	0.58167																	
14	0.76482	-0.125863	0.61117																	
15	0.71690	-0.119885	0.63482																	
16	0.73371	-0.090734	0.59159																	
17	0.71727	-0.064251	0.67599																	
18	0.51054	-0.012939	1.47064																	
19	0.76935	-0.171266	0.49724																	
20	0.65594	-0.071875	0.65304																	
21	0.74182	-0.111105	1.05542																	
22	0.63050	-0.124793	0.59628																	
23	0.79361	-0.105191	0.67072																	
24	0.78975	-0.100437	0.60228																	
25	0.79936	-0.105143	0.57491																	
26	0.87202	-0.134670	0.48496																	

Figure K 2: Options button for performing 2 Sample t test in Minitab

### STEP 3:

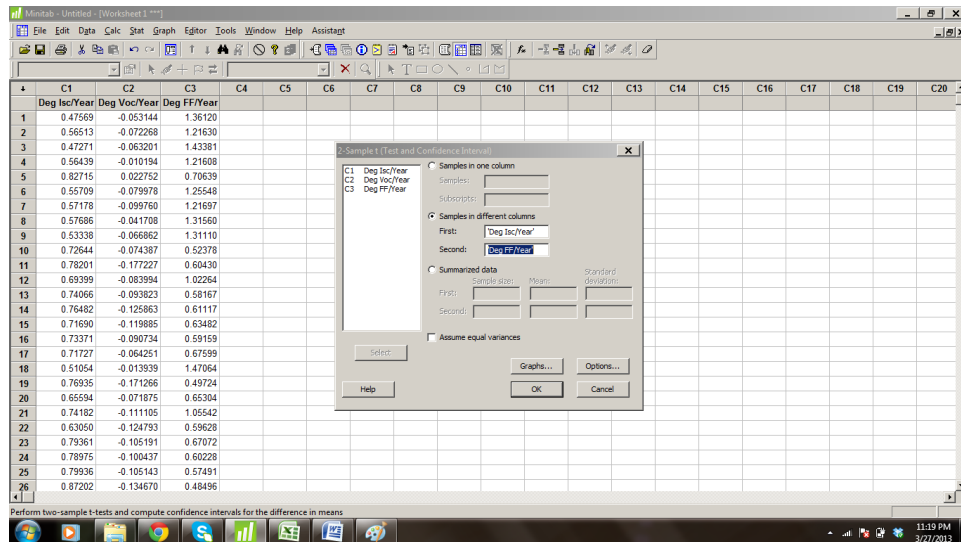


Figure K 3: Samples placed on two different columns in the dialog box are compared

### STEP 4:

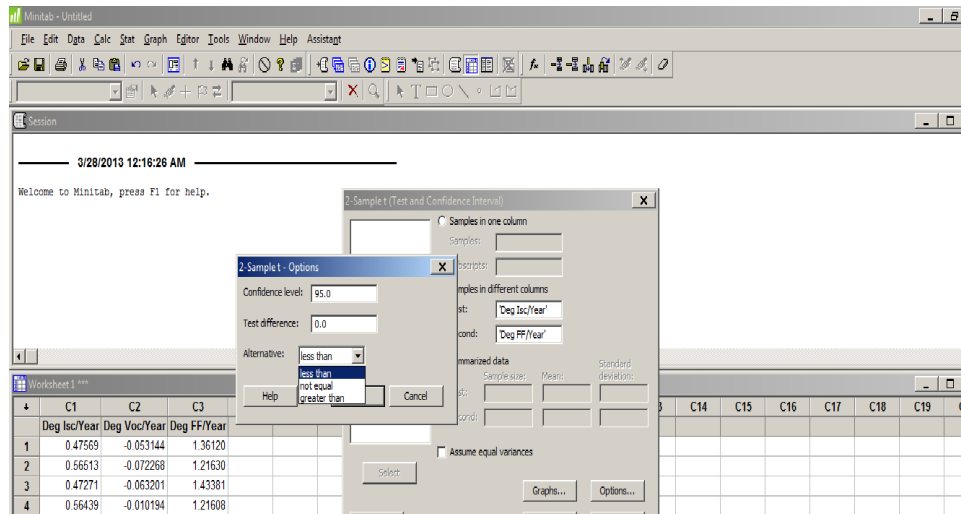


Figure K 4: A symbol chosen for implementing the alternative hypothesis

**STEP 5:** A window pops up with a probability value (P-Value). It is compared with the significance level (0.05). Since the P- Value is less than significance value, the null hypothesis can be rejected and the alternative hypothesis is true.

```

Welcome to Minitab, press F1 for help.

Two-Sample T-Test and CI: Deg Isc/Year, Deg FF/Year

Two-sample T for Deg Isc/Year vs Deg FF/Year

      N    Mean  StDev  SE Mean
Deg Isc/Year  1064  0.666  0.149   0.0046
Deg FF/Year   1064  0.948  0.324   0.0099

Difference = mu (Deg Isc/Year) - mu (Deg FF/Year)
Estimate for difference:  -0.2816
95% CI for difference:  (-0.3031, -0.2601)
T-Test of difference = 0 (vs not =): T-Value = -25.74  P-Value = 0.000  DF =
1493

```

Figure K 5: Window containing the P-Value

The same procedure is followed for implementing the hypothesis testing between Degradation Isc per year and Degradation Voc per year and the statistical factor affecting the power drop could be identified.

The entire procedure is followed for all models in the power plant to identify the major factor causing the power drop.